OPEN ACCESS

Original research

Axon guidance cue SEMA3A promotes the aggressive phenotype of basal-like PDAC

Francesca Lupo,[1] Francesco Pezzini,[1] Davide Pasini,[1,2] Elena Fiorini,[1] Annalisa Adamo,[2] Lisa Veghini,[1] Michele Bevere,[3] Cristina Frusteri,[2] Pietro Delfino,[4,5] Sabrina D'agosto,[4,6] Silvia Andreani ,[3,7] Geny Piro,[8] Antonia Malinova,[1] Tian Wang,[2] Francesco De Sanctis,[2] Rita Teresa Lawlor,[3] Chang-il Hwang ,[9] Carmine Carbone ,[8] Ivano Amelio,[10] Peter Bailey,[11] Vincenzo Bronte ,[2] David Tuveson ,[12] Aldo Scarpa ,[3,4] Stefano Ugel,[2] Vincenzo Corbo [1]

► Additional supplemental material is published online only. To view, please visit the journal online (https://doi.org/10.1136/gutjnl-2023-329807).

For numbered affiliations see end of article.

Correspondence to
Professor Vincenzo Corbo, Department of Engineering for Innovation Medicine, University of Verona, Verona, Veneto, Italy; vincenzo.corbo@univr.it

Received 2 March 2023
Accepted 5 April 2024

To cite: Lupo F, Pezzini F, Pasini D, *et al*. *Gut* Epub ahead of print: [*please include* Day Month Year]. doi:10.1136/gutjnl-2023-329807

ABSTRACT

Objective The dysregulation of the axon guidance pathway is common in pancreatic ductal adenocarcinoma (PDAC), yet our understanding of its biological relevance is limited. Here, we investigated the functional role of the axon guidance cue SEMA3A in supporting PDAC progression.

Design We integrated bulk and single-cell transcriptomic datasets of human PDAC with in situ hybridisation analyses of patients' tissues to evaluate SEMA3A expression in molecular subtypes of PDAC. Gain and loss of function experiments in PDAC cell lines and organoids were performed to dissect how SEMA3A contributes to define a biologically aggressive phenotype.

Results In PDAC tissues, SEMA3A is expressed by stromal elements and selectively enriched in basal-like/squamous epithelial cells. Accordingly, expression of SEMA3A in PDAC cells is induced by both cell-intrinsic and cell-extrinsic determinants of the basal-like phenotype. *In vitro*, SEMA3A promotes cell migration as well as anoikis resistance. At the molecular level, these phenotypes are associated with increased focal adhesion kinase signalling through canonical SEMA3A-NRP1 axis. SEMA3A provides mouse PDAC cells with greater metastatic competence and favours intratumoural infiltration of tumour-associated macrophages and reduced density of T cells. Mechanistically, SEMA3A functions as chemoattractant for macrophages and skews their polarisation towards an M2-like phenotype. In SEMA3A^{high} tumours, depletion of macrophages results in greater intratumour infiltration by CD8+T cells and better control of the disease from antitumour treatment.

Conclusions Here, we show that SEMA3A is a stress-sensitive locus that promotes the malignant phenotype of basal-like PDAC through both cell-intrinsic and cell-extrinsic mechanisms.

WHAT IS ALREADY KNOWN ON THIS TOPIC

⇒ PDAC cell states manifest as a wide range of environmentally contingent traits.
⇒ The PDAC cell state that displays aggressive biological behavior underscores the dysregulation of axon guidance programs.
⇒ Elevated tissue expression of SEMA3A is consistently associated with poor outcome in PDAC.

WHAT THIS STUDY ADDS

⇒ SEMA3A is a stress-sensitive locus that responds to the different microenvironmental challenges of the complex PDAC tumour microenvironment.
⇒ SEMA3A exerts both cell-autonomous and non-cell autonomous effects to sustain PDAC progression and drive resistance to chemotherapy.
⇒ Tumour-derived SEMA3A favours intra-tumoral infiltration of macrophages and exclusion of T cells.

HOW THIS STUDY MIGHT AFFECT RESEARCH, PRACTICE OR POLICY

⇒ CD8+T cells play a dominant role in controlling the disease in the setting of SEMA3A+ tumours, which might be exploited therapeutically.
⇒ A comprehensive investigation of the mechanisms enabling cancer cells to break through several microenvironmental constraints will help to achieve a better PDAC control.

INTRODUCTION

Pancreatic ductal adenocarcinoma (PDAC) is a malignancy of the exocrine pancreas and the deadliest cancer worldwide.[1] Most patients present with an unresectable disease at diagnosis that is treated with chemotherapy-based regimens.[2] Overall, PDAC is poorly responsive to available treatments.[2] Evidence from studies addressing recurrences of PDAC following radical surgery suggests that pancreatic cancer is a systemic disease at presentation.[3–5] As it stands, understanding the mechanisms of tumour progression and dissemination in PDAC is vital to improve patients' outcomes in the long term. At histopathological level, PDAC tissues feature a prominent stromal reaction, abundant cancer-associated fibroblasts (CAFs) and macrophages, with T cells typically excluded. Expression

profile analyses have evidenced two main subtypes of PDAC cells.[6–9] These alternative cell states are not permanently encoded but rather defined by the integration of cell intrinsic (eg, specific allelic statuses) and cell extrinsic (eg, microenvironmental cues) factors.[10 11] Moreover, PDAC tissues often show the coexistence of both basal-like and classical cells within the same tumour,[7 12] which can be partially explained by the existence of spatially confined subtumour microenvironments (TMEs).[13] Of the two epithelial PDAC cell states, the basal-like/squamous subtype is characterised by the loss of pancreatic endodermal identity and shows a more aggressive biological behaviour.[6 9] Accordingly, basal-like/squamous cells accumulate in the advanced stages of the disease.[7] Molecular signatures indicative of a challenging microenvironment (eg, hypoxia, fibrosis) represent core gene programmes of this subtype.[6 7] This aligns with the possibility of inducing the basal-like/squamous subtype *ex vivo* by integrating specific TME cues into the culture medium.[11]

Genetic and epigenetic dysregulation of the Axon guidance pathway have been consistently reported in PDAC.[14–16] Recently, Krebs *et al* showed the enrichment of axon guidance-associated gene sets in basal-like as well as high-grade PDAC.[17] Furthermore, neuronal-like progenitor cell states have been reported in undifferentiated tumours[18] and are positively selected in post-treatment tumours.[12] Most of the previous studies have focused on investigating the role of members of the Slit/Robo axis on the PDAC malignant traits as well as its cell identity.[17 19–22] Semaphorins are the largest family of axon guidance cues, which were originally identified as chemorepellent proteins in the nervous system.[23 24] SEMA3A is a class 3 semaphorin, that is, secreted, whose elevated tissue expression is a negative prognostic marker in PDAC.[14 15] Nonetheless, the functional role of semaphorins in PDAC remains to be elucidated. Here, we investigated whether the semaphorins signalling pathway contributes to shaping aggressive PDAC phenotypes. Integrating bulk and single-cell RNA-sequencing data with in situ analysis of PDAC tissues, we demonstrated that *SEMA3A* expression is prominent in the stroma of PDAC and specifically enriched in the epithelial cells of the basal-like/squamous subtype. We found that both cell-intrinsic and cell-extrinsic factors promoting the basal-like/squamous subtype induce expression of SEMA3A in PDAC cells. Mechanistically, SEMA3A acts cell autonomously to promote mesenchymal-like traits, including anoikis resistance, through the activation of focal adhesion kinase (FAK). In vivo, SEMA3A promotes the intratumour infiltration of macrophages and reduces the density of T cells. Finally, the depletion of macrophages with a CSF1R monoclonal antibody improved gemcitabine antitumour activity, particularly for SEMA3A expressing tumours.

RESULTS

The expression of class 3 semaphorins is associated with the basal-like/squamous phenotype of PDAC

The interrogation of three distinct PDAC transcriptomic datasets[6 7 25] revealed that the expression level of four semaphorins significantly discriminated basal-like from classical tumours in the ICGC[6] and the PanCuRx[7] cohorts (figure 1A, online supplemental figure S1A). *SEMA4G* levels were enriched in classical tumours while the expression of *SEMA3A*, *SEMA3C* and *SEMA3F* was significantly enriched in basal-like PDAC. Furthermore, *SEMA3A* and *SEMA3C* showed the highest correlation with basal-like/squamous transcriptional signatures, including those indicative of a challenging microenvironment (eg, hypoxia and fibrosis) and of epithelial-to-mesenchymal transition (EMT) (figure 1B, online supplemental figure S1B). Therefore, we decided to focus on SEMA3A and SEMA3C. We identified higher SEMA3A expression in whole cell lysates from cells with prominent squamous features including expression of TP63/ΔNp63 (Colo357, L3.6pl, BxPC3 and MiaPaCa2) (figure 1C). Similarly, SEMA3A expression was higher in patient-derived organoids (PDOs) that classify as basal-like/squamous (figure 1C and online supplemental figure S1C). SEMA3C showed a more promiscuous pattern of expression in human cell lines and PDOs (figure 1C). Transient downregulation of *p63* was sufficient to reduce SEMA3A but not SEMA3C expression in MiaPaCa2 and BxPC3 cell lines (figure 1D). To understand the modulation of SEMA3A and SEMA3C expression during PDAC progression, we examined their expression levels across mouse PDAC cells displaying different *Trp53* allelic statuses, derived from tissues at different stages of disease progression. Overall, the expression level of both *Sema3a* and *Sema3c* was variable among stage-matched organoid cultures (ie, PanIN, tumour and metastases) from the KC (*Kras*$^{LSL\text{-}G12D/+}$;*Pdx-1*-Cre) and KPC (*Kras*$^{LSL\text{-}G12D/+}$;*Trp53*$^{LSL\text{-}R172H/+}$;*Pdx-1*-Cre) mouse models[26 27] (online supplemental figure S1D). However, we found a trend towards an increase of *Sema3a* expression in advanced-stage cultures, and a significant difference between mM (ie, metastatic) and mN (ie, normal pancreas) cultures (online supplemental figure S1D) also in terms of protein expression and secretion (online supplemental figure S1E).

Our data also suggest that the loss of heterozygosity (LOH) of *Trp53* licenses SEMA3A expression in mouse PDAC cells (figure 1E, online supplemental figure S1F–H). In mouse PDAC, the in vivo progression towards invasive tumours is almost invariably associated with loss of heterozygosity (LOH) of *Trp53*.[27–30] In human PDAC, the biallelic inactivation of *P53* is significantly enriched in basal-like/squamous tumours.[6] mT organoid cultures established from KPC mice, differently from mM organoids, contain cells that retain the wild-type copy of *Trp53*.[28 29] To deplete *Trp53* wild-type cells, we treated mT6 with 10 µM of Nutlin-3A[31] (online supplemental figure S1F). Loss of the wild-type copy of *Trp53* in Nutlin-3A treated mT6 was associated with increased transcriptional and protein expression of SEMA3A, while levels of SEMA3C were unaffected (figure 1E, online supplemental figure S1G). Moreover, only in tumour organoids displaying LOH of *Trp53*, we could observe a significant induction of *Sema3a* expression following forced expression of p63 (figure 1E). To corroborate our findings, we leveraged mouse PDAC cell lines (referred to as KP^{sh}[32]) where the loss of *Trp53* is contingent on the doxycycline-induced expression of a shRNA targeting *Trp53*. The genetic inactivation of *Trp53* in these cell lines led to a significant upregulation of *Sema3a* expression (online supplemental figure S1H). In line with the human data, forced expression of *p63* in the KPC cell line FC1199, which displays *Trp53* biallelic inactivation (online supplemental figure S1I), increased *Sema3a* expression (figure 1F). This was associated with increased occupancy of *Sema3a* promoter by p63 (figure 1F, online supplemental figure S1J). Conversely, transient downregulation of mutant *Kras* in KPC cell lines did not lead to changes in *Sema3a* expression while reducing the levels of genes downstream of mutant KRAS signalling such as *Nq01* and *Sema3c*[33 34] (online supplemental figure S1K).

Environmental cues induce the expression of SEMA3A in mouse PDAC cells

Next, we investigated whether microenvironmental pressures that can lead to the basal-like cell state affected SEMA3A/3C

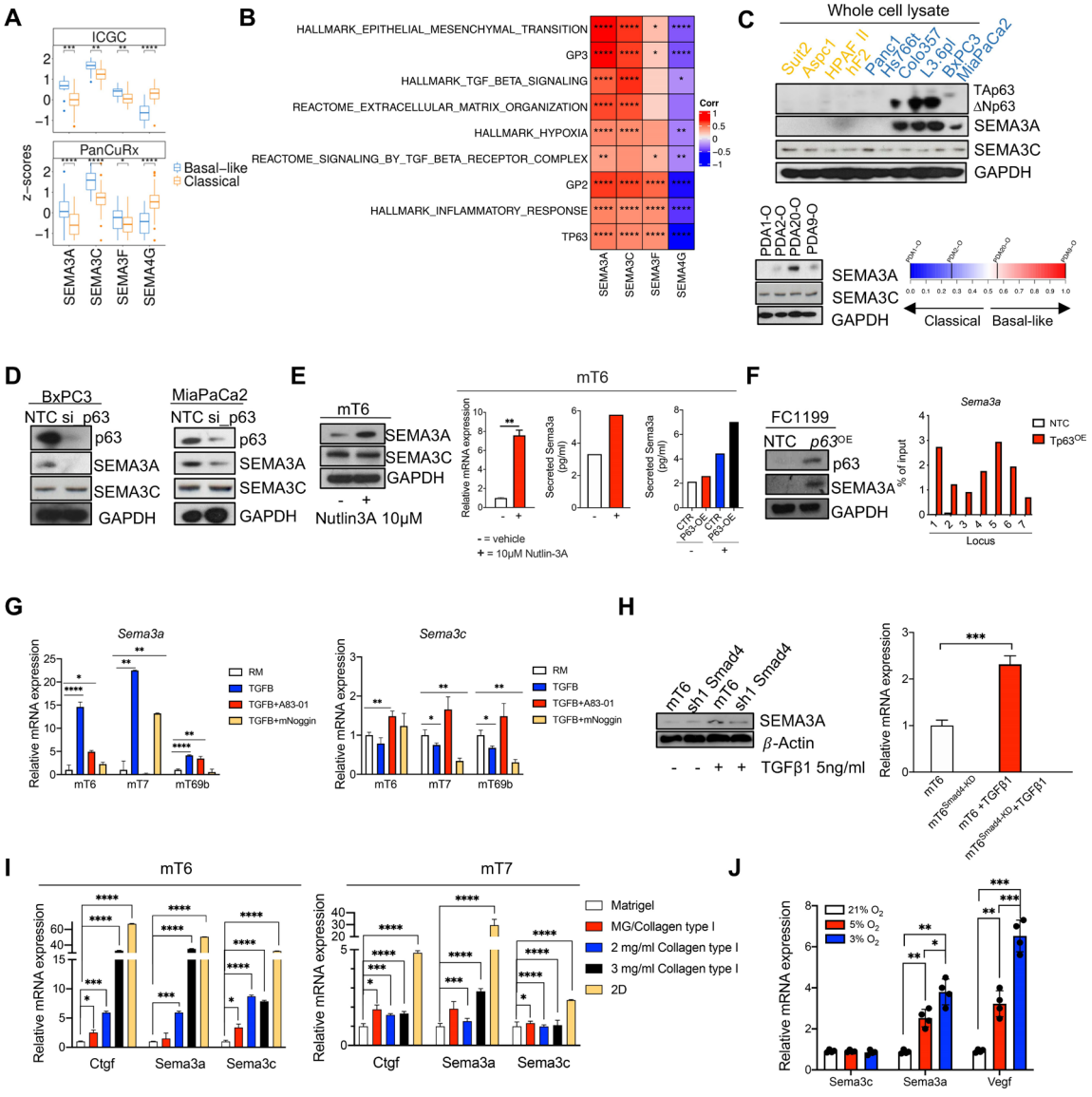

Figure 1 Cell intrinsic and cell extrinsic inputs eliciting SEMA3A expression in PDAC cells. (A) Boxplot of *SEMA3A*, *SEMA3C*, *SEMA3F* and *SEMA4G* Z-scores stratified by the Moffitt subtypes[9] in the ICGC,[6] and the PanCuRx[7] cohorts. **p<0.01, ***p<0.001, ****p<0.0001 by Student's t-test. (B) Heatmap showing correlation (Spearman's correlation) between the indicated semaphorins and basal-like/squamous associated gene programmes in the ICGC cohort. GP2 and GP3 refers to the core gene programmes defining the squamous subtype in Bailey *et al*.[6] All annotated boxes, p<0.05. (C) Upper panel, immunoblot analysis of p63, SEMA3A and SEMA3C in whole cell lysates of different human pancreatic cancer cell lines. Lower panel, immunoblot analysis of SEMA3A and SEMA3C in whole cell lysates of primary tumour organoids ordered based on their basal-like identity (from left to right increasing basalness). GAPDH, loading control. (D) Immunoblot analysis of p63, SEMA3A and SEMA3C in whole cell lysates from BxPC3 (left) and MiaPaCa2 (right) squamous cell lines transfected with either non-targeting control (NTC) of siRNA targeting p63. GAPDH as loading control. (E) Left panel, immunoblot analysis of SEMA3A and SEMA3C in whole cell lysates from mT6 treated with vehicle or Nutlin-3A (see the 'Methods' section). GAPDH, loading control. Changes in the expression (qPCR) or secretion (ELISA) of SEMA3A were detected in mT6 following Nutlin-3A treatment (right panel). (F) Immunoblot analysis of p63 and SEMA3A in KPC 2D cell lines (FC1199) transduced with either an empty vector (NTC) or a p63 ORF. On the right, anti-p63 ChIP-qPCR analysis of seven different genomic regions upstream of the promoter of *Sema3a*. The ChIP-qPCR signal of each sample was normalised to its own input. (G) qPCR showing changes in the expression of *Sema3a* (left) and *Sema3c* (right) relative to the reduced media condition (RM, without A83-01 and mNoggin) in three different tumour organoid cultures treated as indicated. Data are mean of three technical replicates. ****p<0.0001, **p<0.01, *p<0.05 by unpaired Student's t-test. (H) Immunoblot analysis of SEMA3A in whole cell lysates from SMAD4 proficient and deficient mT6 organoids that were treated with either vehicle or TGF-β1 for 48 hours. β-actin was used as loading control (left panel). qPCR analysis (right panel) of SEMA3a in mT6 organoids treated as indicated. ***p<0.001 by Student's t-test. (I) Changes in the expression of *Ctgf*, *Sema3a* and *Sema3c* in mouse tumour organoids (n=2) grown on substrate of increasing rigidity for 48 hours. Data are represented as mean value±SD (n=3 technical replicates). *p<0.05, ***p<0.001, ****p<0.0001 by Student's t-test. (J) Changes in the expression levels of *Sema3c, Sema3a* and *Vegf* in mouse tumour organoids cultivated under different O_2 concentration for 24 hours. Results are shown as mean±SD of four independent experiments. ***p<0.001, **p<0.01, *p<0.05 by Student's t-test. GAPDH, glyceraldehyde 3-phosphate dehydrogenase.

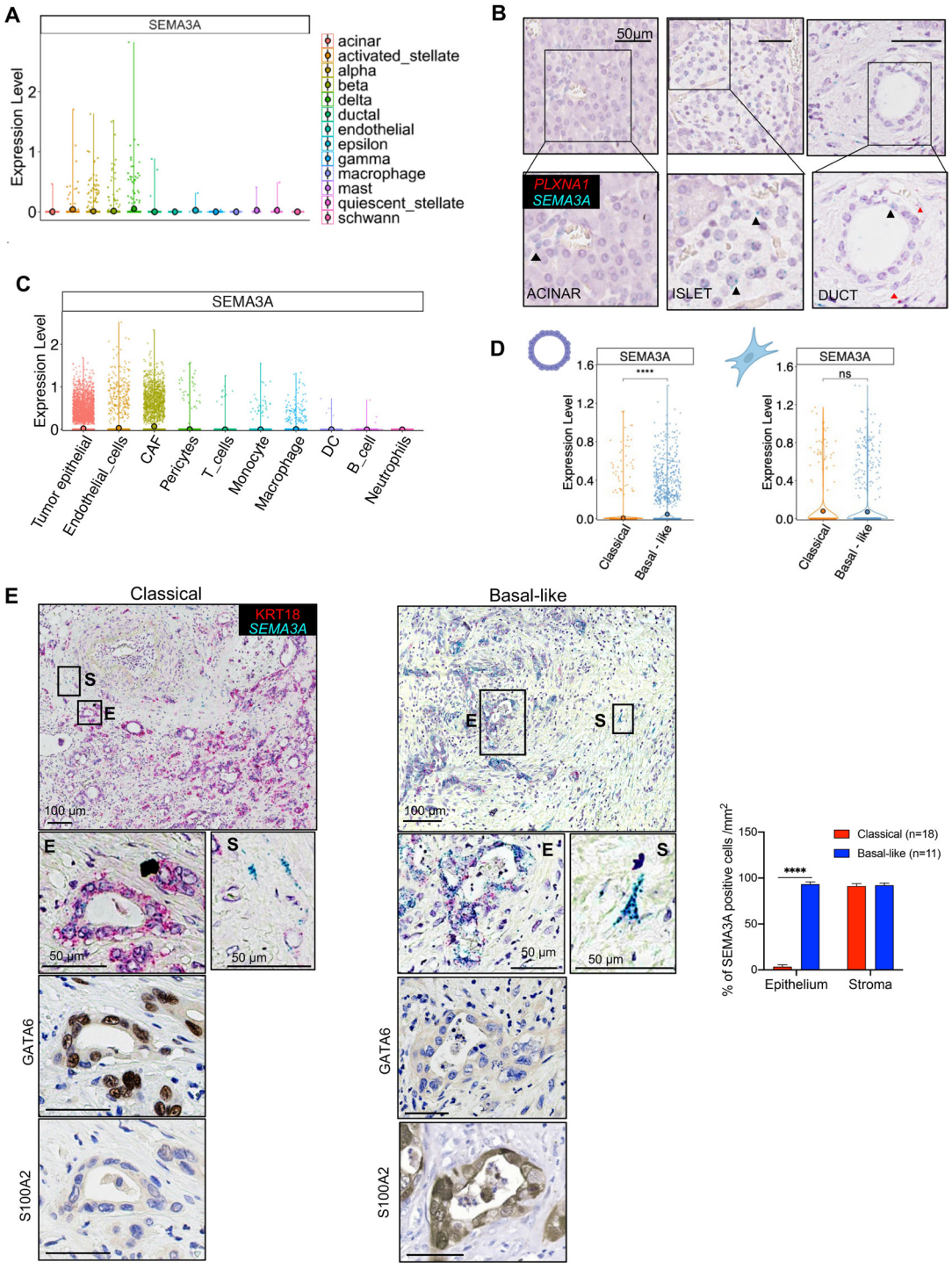

Figure 2 SEMA3A expression is selectively enriched in basal-like PDAC. (A) Violin plots of the normalised expression of *SEMA3A* in each annotated cell cluster from the integration of four different scRNA-Seq datasets[35–38] of normal pancreatic tissues (see the 'Methods' section). (B) Representative ISH images showing rare *SEMA3A* (green) and *PLXNA1* (red) signals in acinar cells (left panel), islet cells (middle panel) and ductal cells (right panel). Scale bar, 50 µm. Insets show magnification of selected areas with visible signals for *SEMA3A* (black arrowheads) or *PLXNA1* (red arrowheads). (C) Violin plots of the normalised expression of *SEMA3A* in each annotated cell cluster from the integration of 4 different scRNA-Seq datasets[7 40–42] of pancreatic cancer tissues (see the 'Methods' section). (D) Epithelial and fibroblasts expression of *SEMA3A* in individual cells from PDAC cases almost exclusively composed by either classical or basal-like cells (see online supplemental figure S2H). ****p<0.0001 and ns, not significant by Wilcoxon and Mann-Whitney. (E) Left panel, representative ISH images showing expression of *SEMA3A* in the epithelial (CK18+) and stromal (CK18–) compartment of a pancreatic cancer tissue subdomain classified as classical based on expression of GATA6. Right panel, representative ISH images showing expression of *SEMA3A* in the epithelial and stromal compartment of a tumour area classified as basal-like based on the expression of S100A2 and lack of GATA6 expression. Scale bars as indicated. Quantification is provided as percentage of positive cells (see also online supplemental figure S3B) in the selected area. ****p<0.0001 by unpaired Student's t-test. ISH, in situ hybridisation.

expression. Three different mT cultures (mT6, 7, 69) grown in the presence of recombinant TGF-β1 (see methods) invariably showed increased *Sema3a* expression, while a context-dependent effect was observed for *Sema3c* (figure 1G). The stimulatory effect of TGF-β1 on *Sema3a* expression could be blocked either pharmacologically (figure 1G) or by the genetic downregulation of SMAD4 (figure 1H, online supplemental figure S1L). Matrix rigidity also affected Semaphorins expression. The cultivation of two different mTs (mT6 and mT7) in matrices of increasing rigidity significantly induced the expression of the mechanosensitive gene *Ctgf* as well as of *Sema3a* and *Sema3c,* although to a different extent (figure 1I). Finally, lowering the concentration of O_2 significantly induced a dose-dependent expression of the hypoxia-responsive gene *Vegf*, of *Sema3a,* but not of *Sema3c* in FC1199 (figure 1J). Altogether, our results show that *Sema3a* is responsive to both cell intrinsic and cell extrinsic inputs that define aggressive PDAC phenotypes. These findings prompted us to investigate whether and how SEMA3A contributes to shape aggressive PDAC phenotypes.

SEMA3A expression in normal and malignant pancreatic tissues

Elevated tissue expression of SEMA3A has been previously linked with dismal outcomes in PDAC.[14] Here, we sought to clarify the major cellular sources of SEMA3A in pancreatic tissues. Integration of available scRNA-Seq data[35–38] with in situ hybridisation (ISH) analysis of normal pancreatic tissues revealed that rare epithelial cells (mostly neuroendocrine cells) express low levels of *SEMA3A* and its receptor *PLXNA1* (figure 2A,B). Accordingly, the analysis of bulk transcriptomic data revealed that levels of *SEMA3A* were significantly higher in tumour versus normal pancreatic tissues[39] (online supplemental figure S2A). To specifically link epithelial SEMA3A expression to molecular features of aggressive PDAC, we leveraged the transcriptomic data of the PanCuRx cohort which were generated following laser-capture microdissection of the epithelial compartment.[7] Samples were stratified based on the *SEMA3A* expression status (either high or low, see the 'Methods' section). *SEMA3A*^{high} tumours were enriched for basal-like subtypes (online supplemental figure S2B) and major imbalances of the mutant *KRAS* allele (online supplemental figure S2C).

To further corroborate the link between *SEMA3A* expression in epithelial cells with the basal-like transcriptional cell state, we interrogated scRNA-Seq data of human PDAC tissues.[7 40–42] Following harmonisation of the four datasets,[43] cell type annotation was performed using singleR[44] and the Human Primary Cell Atlas[44] (online supplemental figure S2D). As expected, epithelial and stromal cells represented the most populated cell clusters. Next, we inferred copy-number alterations[45] in the ductal cell clusters to identify malignant cells and exclude normal epithelial cells (online supplemental figure S2E). CAFs were annotated in the stromal cell clusters by post hoc analysis using known gene signatures[46] (online supplemental figure S2F). *SEMA3A* expression was not restricted to epithelial cells but rather prominent in stromal elements (figure 2C). Expression of SEMA3A receptor (*PLXNA1*) and coreceptor (*NRP1*) was rather promiscuous in PDAC tissues, which suggests that many cell types might be responsive to this axon guidance cue (online supplemental figure S2G). When considering cases with the highest proportion of basal-like and classical cells across the four datasets (online supplemental figure S2H), significant differences in terms of *SEMA3A* expression were restricted to the malignant epithelium (figure 2D). In scRNA-seq data from an autochthonous mouse model of PDAC,[47] *Sema3a* expression was higher in the epithelial compartment and particularly enriched in basal-like cells (online supplemental figure S2I). Finally, we performed ISH for *SEMA3A* on human PDAC tissues (n=29) and classified neoplastic cells as either classical or basal-like/squamous based on the expression of markers of the two subtypes (online supplemental figure S3A). As expected, PDAC tissues displayed marked intratumour heterogeneity with coexistence of basal-like and classical neoplastic cells (online supplemental figure S3A). For each tumour tissue, we identified 1 mm^2 area exclusively occupied by either classical or basal-like/squamous cells and evaluated *SEMA3A* in the epithelial and stromal compartments. In keeping with the scRNA-Seq data, *SEMA3A* was almost exclusively detected in basal-like epithelial cells while detectable in stromal elements surrounding both classical and basal-like cells (figure 2E and online supplemental figure S3B). In sum, our analysis shows that *SEMA3A* expression is not restricted to epithelial cells in PDAC tissues, yet it is mostly confined to basal-like/squamous epithelial cells. Therefore, we sought to investigate the role of tumour cells derived SEMA3A in pancreatic progression.

SEMA3A activates the PI3K/Akt signalling pathway in mouse PDAC cells

To understand whether and how dysregulated SEMA3A levels contribute to promote malignancy of PDAC cells, we performed genetic perturbation experiments using both mouse PDAC cell lines and organoids. KPC-derived cell lines (FC1199, FC1245 and FC1242) display mesenchymal-like features (online supplemental figure S4A) and high levels of *Sema3a*. Therefore, we derived subclones displaying a reduced expression of the gene (online supplemental figure S4B). *Sema3a*^{low} FC1199 and FC1245 subclones (designated by the B suffix) and mT6 organoids were stably transduced with a vector carrying an open-reading frame for *Sema3a* (figure 3A,B and online supplemental figure S4C,D). Cas9-expressing mM3L organoids and *Sema3a*^{high} FC1199 and FC1245 monolayer cell cultures (designated by the A suffix) were transduced with two different gRNAs targeting *Sema3a* (figure 3A,C and online supplemental figure S4C,E). Genetic manipulation of *Sema3a* also resulted in coherent changes in the level of the secreted proteins in the cultures conditioned media (online supplemental figure S4F). No difference in cell viability over the course of 7 days was observed for mouse organoids (figure 3D) as well as for 2D cultures (figure 3E,F) displaying different levels of *Sema3a*.

Next, we evaluated whether the dysregulation of *Sema3a* in mouse PDAC cells affected fluxes through the major signalling pathways, that is, MAPK and PI3K/Akt pathways. To test the effect of the culturing medium on pathways' modulation, we cultured organoids (mT6 and mM3L) in standard and minimal media (depleted of growth factors and TGF-β inhibitors). Regardless of the culturing media, SEMA3A promoted activation of the PI3K/Akt pathway in organoids (figure 3G,H). Similar changes were observed in monolayer cell cultures following S*ema3a* perturbation (figure 3I). Conversely, the effect of *Sema3a* dysregulation on the activation of the MAPK pathway was variable across cultures and culture conditions (online supplemental figure S4G–J). Overall, our data suggest that SEMA3A promotes PI3K/Akt activation in mouse PDAC cultures independently of the culture environment and matrix dimensionality.

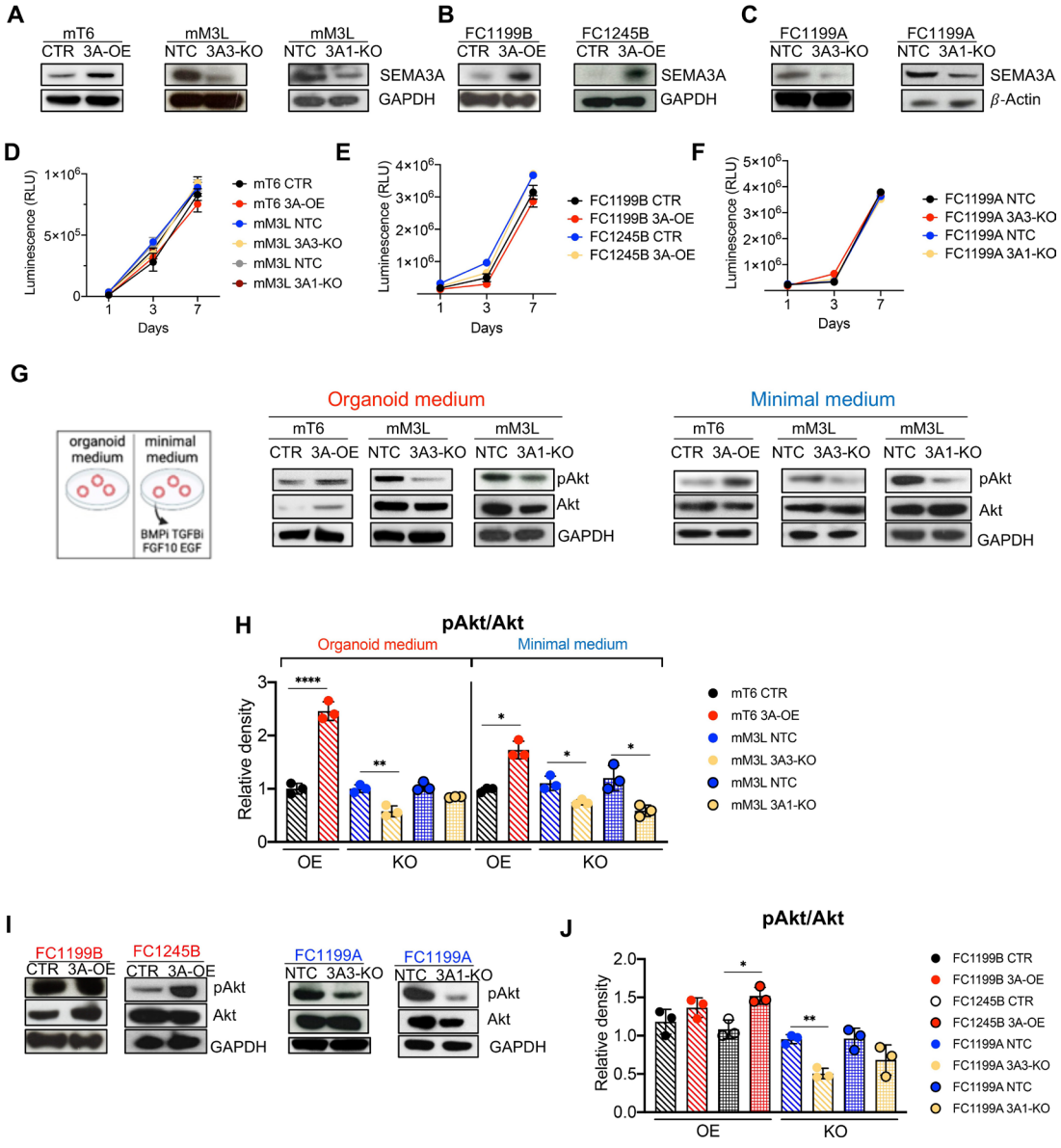

Figure 3 SEMA3A promotes the activation of PI3K/Akt in mouse pancreatic ductal adenocarcinoma (PDAC) cells. (A–C) Immunoblot analyses of SEMA3A in whole cell lysates from mouse tumour (mT6) organoids, mouse metastatic (mM3L) organoids and KPC 2D cell lines (FC1199 and FC1245) following either overexpression (OE) or genetic knockout (KO); GAPDH was used as loading control in A and B while β-actin was used in C. (D–F) Proliferation (as total luminescence) measured over the course of 7 days of either cell lines or organoid cultures from A to C. The suffix L for mM3 denotes that the culture was established from a liver metastasis. The suffixes A and B for FC1199 and FC1245 denote clonal populations displaying high and low levels of SEMA3A, respectively. NTC or CTR denotes cultures stably transduced with a mock control. (G) Immunoblot analyses of the indicated proteins in whole cell lysates from mouse organoid cultures (mT6 and mM3L) cultivated in either organoid medium or in minimal medium. GAPDH was used as loading control. (H) Bar plots showing the quantification of changes in the phosphorylated levels of p-AKT as relative density of the total protein level. Data are presented as means±SD of three biological replicates. ****p<0.0001, **p<0.01, *p<0.05 by Student's t-test corrected for multiple comparison using the Holm-Sidak method. (I) Immunoblot analyses of the indicated proteins in whole cell lysates from mouse pancreatic cancer cell lines following either overexpression (OE) or genetic knockdown (KO) of SEMA3A. GAPDH was used as loading control. (J) Bar plots showing the quantification of changes in the phosphorylated levels of p-AKT as relative density of the total protein level. Data re presented as means±SD of three biological replicates. **p<0.01, *p<0.05 by Student's t-test corrected for multiple comparison using the Holm-Sidak method. GAPDH, glyceraldehyde 3-phosphate dehydrogenase.

SEMA3A promotes increased migration, anoikis resistance and increases lung metastases

Expression of SEMA3A in human PDAC tissue correlates with EMT gene programmes (figure 1B), and transcription of *Sema3a* in mouse cultures is induced by TGF-β1 (figure 1H). In organoid cultures, the modulation of *Sema3a* was associated with significant changes in mesenchymal (Vimentin) or epithelial (E-cadherin) markers only in a minimal medium (online supplemental figure S5A,B). Furthermore, neither the knockout nor the overexpression of *Sema3a* significantly influenced TGF-β1 induction of EMT transcription factors expression in organoids (online supplemental figure S5C,D). As expected, TGF-β1 failed to induce *Sema3a* transcription in knockout cells (online supplemental figure S5D). In monolayer cell cultures (FC1199 and

FC1245), modulation of *Sema3a* had no significant effect on the expression of EMT markers (online supplemental figure S5E,F).

Next, we asked whether SEMA3A functionally contributes to EMT traits in mouse PDAC cells. The manipulation of *Sema3a* expression in mouse PDAC cultures had a significant effect on their migratory capability (figure 4A). The wound healing assay showed that *Sema3a* significantly promoted the migration of FC1199B cells (figure 4A). In keeping with that, the treatment with recombinant SEMA3A rescued the effect of gene knockout on the migratory capacity of FC1199A cells (figure 4A, right panel). Next, we set up an anoikis assay for both monolayer cell cultures and organoids (see methods). The depletion of *Sema3a* from mM organoids significantly increased apoptotic cell death (figure 4B). Similar to the anoikis inhibitor Y27632 (Rho-associated kinase inhibitor, RhoKi), exogenous supplementation of recombinant SEMA3A significantly reduced apoptotic cell death. In keeping with that, overexpression of *Sema3a* in FC1199 significantly reduced cell death of cells grown in suspension (figure 4C). To test whether the resistance to anoikis was mediated by the canonical SEMA3A-NRP1 axis, we measured the anti-anoikis effect of SEMA3A following silencing of either *Nrp1* or the main coreceptor *Plxna1* (online supplemental figure S5G). Silencing of *Nrp1,* and to a lesser extent of *Plxna1,* significantly prevented the protective effect of SEMA3A against anoikis (online supplemental figure S5G). FAK is an important regulator of cell survival with an established role in mediating anoikis resistance.[48] We found that cancer-cell-derived SEMA3A induces activation of FAK (autophosphorylation at Tyr 397) (figure 4D), which was instead reduced on silencing of SEMA3A receptors (online supplemental figure S5H). Of note, silencing of SEMA3A receptors, particularly of PLXNA1, reduced fluxes through main signalling pathways (online supplemental figure S5H). Treatment of mouse PDAC cultures with recombinant SEMA3A stimulated FAK autophosphorylation (figure 4E) and FAK inhibition with the selective inhibitor defactinib (FAKi) counteracted the SEMA3A protective effect against anoikis (figure 4F and online supplemental figure S5I). Anoikis resistance is a hallmark of metastatic cells.[49] Therefore, we injected both *Sema3a* proficient and deficient cells directly into the circulation to model postintravasation steps of the metastatic process, including survival into the circulation. In accordance with the in vitro experiments, *Sema3a* proficient cells rapidly colonised the lung parenchyma as opposed to *Sema3a* deficient cells (figure 4G). Overall, our data suggest that *Sema3a* is dispensable for the induction of an EMT transcriptional phenotype driven by microenvironmental cue (eg, TGF-β); however, it is an important mediator of mesenchymal-like traits in PDAC.

SEMA3A expression sustains basal-like/squamous gene programmes in PDAC

To identify pathways downstream of *Sema3a* involved in promoting PDAC aggressiveness, we performed transcriptomic analysis on mouse PDAC cells of different genotypes. The overexpression of *Sema3a* had significant effects on the transcriptome of FC1199B with over 2000 genes significantly upregulated and downregulated (figure 5A, online supplemental table S1). The genetic knockout of *Sema3a* led to a similar degree of transcriptomic changes (figure 5D, online supplemental table S3). As shown in figure 5A, the forced overexpression of *Sema3a* was associated with the significant downregulation of *Grem1*, a BMP inhibitor that has been shown to promote epithelialisation of mesenchymal PDAC cells.[50] Next, we performed gene set enrichment analysis on the list of differentially expressed genes using the GSEA method[51] (figure 5B,E). Following the overexpression of *Sema3a*, we observed the enrichment of gene programmes related to cytoskeleton remodelling and the activity of Rho GTPases (figure 5B, online supplemental table S2). In keeping with that, the knockout of *Sema3a* led to the reduced representation of the same gene programmes (figure 5E, online supplemental table S4). Secreted SEMA3A generally induces growth cone collapse in neurons by acting as either chemorepellent or chemoattractant through microtubule and actin reorganisation.[52] Moreover, SEMA3A is reported to interact directly or indirectly with multiple GTPases, including Rho GTPases.[52] Of note, overexpression of *Sema3a* was also associated with a reduced representation of axon guidance gene sets, which we linked to the reduced expression of Slit/Robo genes. When looking at signatures of aggressive human PDAC, we found that SEMA3A^{high} cells presented higher 'squamousness' than SEMA3A^{low} cells. Furthermore, SEMA3A deficient cell lines showed a significant reduction of the GP3 gene programmes defined by Bailey *et al*[6] based on inferred activity of the TGF-β pathway (figure 5C,F). Moreover, gene programmes related to EMT, the TGF-β pathway, the activation of FAK, Rho GTPases and wound healing were significantly enriched in *SEMA3A-high* tumours both in the ICGC[6] and the PanCuRx[7] cohorts (figure 5G,H, online supplemental tables S5–S8).

SEMA3A promotes PDAC progression in vivo

Next, we sought to assess the in vivo phenotypic consequences of *Sema3a* dysregulation. First, we evaluated whether and how SEMA3A influenced tumour growth pattern and kinetics. Overall, *Sema3a* expressing cell lines (FC1199A and FC1245) generated larger tumours with a solid growth pattern as opposed to the cystic pattern observed for *Sema3a* deficient or low cells (figure 6A, online supplemental figure S6A,B). Moreover, 2 out of 11 mice transplanted with *Sema3a* deficient FC1199 cells did not show any detectable mass while tumour masses invariably developed from *Sema3a* expressing cells (figure 6A). Furthermore, SEMA3A expressing tumours (from FC1199 cells) colonised the liver parenchymal more efficiently than the knockout cells after intrasplenic injection (figure 6B).

Next, we generated grafts based on the transplantation of mouse organoids. Immunocompetent mice transplanted with syngeneic organoid cultures display delayed kinetics of in vivo tumour progression as opposed to PDAC established from monolayer cell cultures.[28 29 53] Nonetheless, this model system permits a better evaluation of the effect of genetic perturbation on tumour progression in vivo.[28 54] *Sema3a* deficient mM3L organoids generated smaller tumours in an immunocompetent host (figure 6C and online supplemental figure S6C) while no difference in tumour growth kinetics was observed in immunodeficient hosts (figure 6C). These results suggest the involvement of the immunity in mediating the in vivo protumourigenic effects of SEMA3A in this model system. RNA-Seq analysis of tumour tissues collected at endpoint from mice transplanted with 2D cell lines did not reveal striking transcriptomic changes between the two groups (online supplemental figure S6,D, online supplemental table S9). However, gene-set enrichment analysis showed the overrepresentation of terms related to inflammation and interferon-related pathways in tumours lacking SEMA3A (figure 5D, online supplemental table S10). The characterisation of the immune microenvironment in murine pancreatic tumours established from cells displaying different *Sema3a* statuses suggested profound remodelling of the TME by tumour-derived SEMA3A (figure 6E,F and online supplemental figure S6E,F).

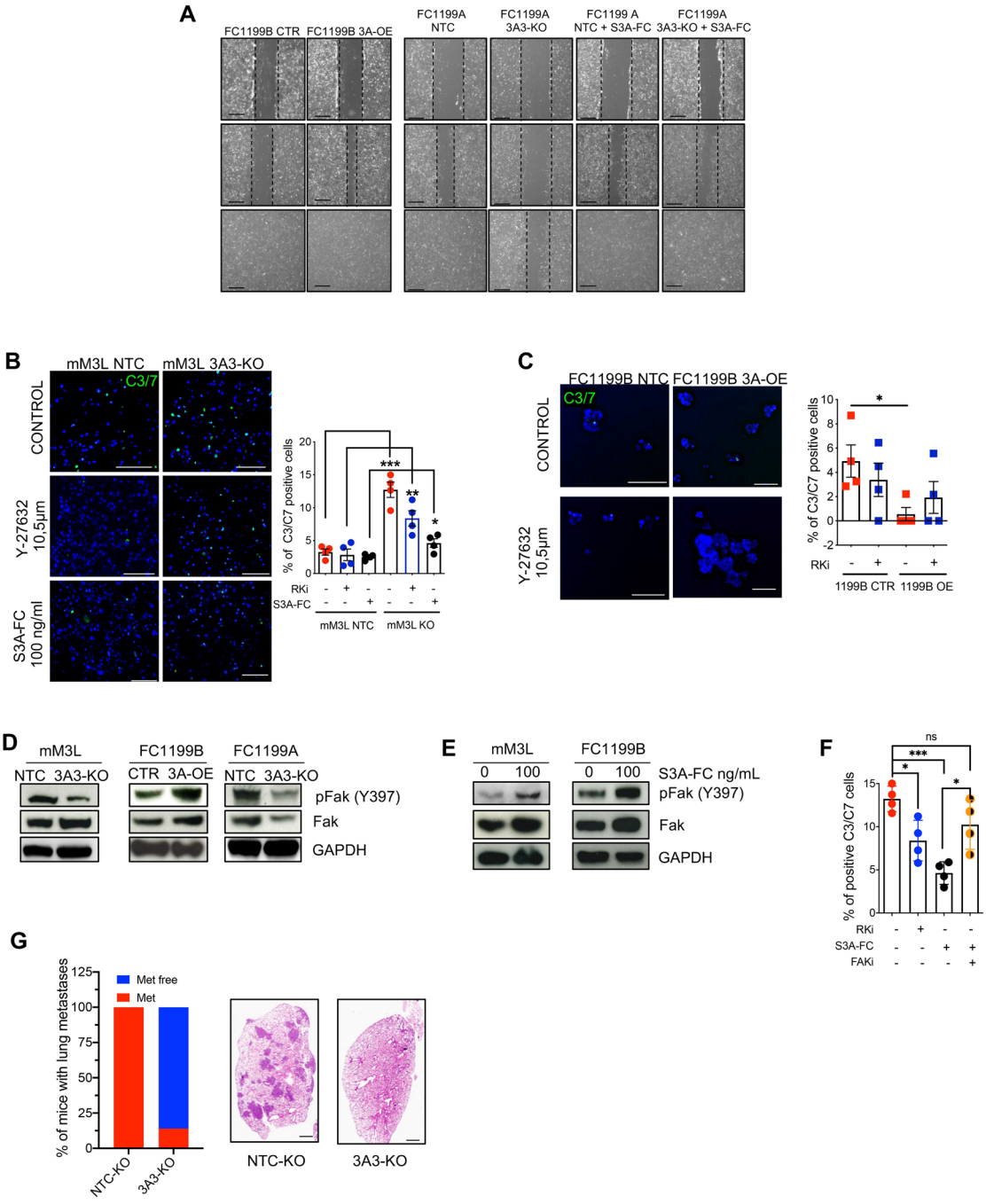

Figure 4 SEMA3A promotes anoikis resistance and increases lung metastases. (A) Representative photographs of the wound area taken immediately after (0), 8 and 24 hours after the incision for FC1199A and B cell lines stably transduced with either non-targeting or control vectors (NTC, CTR), SEMA3A ORF (OE) or gRNAs targeting SEMA3A (KO). FC1199A NTC and KO cells were also treated with recombinant SEMA3A. The experiment was performed in quadruplicate. (B) Representative immunofluorescence images of the anoikis assay (see methods) performed on poly-HEMA coated plate for mM3L NTC and KO treated vehicle (Control), with a RhoK inhibitor (Y-27632), or with recombinant SEMA3A (S3A-FC). Scale bars, 100 µm. Quantification of four independent experiments is provided in the box plot on the right. ***p<0.001, **p<0.01, *p<0.05 by Student's t-test. (C) Representative immunofluorescence images of the anoikis assay (see the 'Methods' section) performed for FC1199B CTR and OE treated with vehicle (Control) or a RhoKi. Scale bars, 100 µm. Quantification of four independent experiments is provided in the box plot on the right. *p<0.05 by Student's t-test. (D) Immunoblot analysis of phospho-FAK, and total FAK in whole cell lysates from mM cultures and KPC cell lines with different SEMA3A genotypes (eg, KO or OE). (E) Immunoblot analysis of phospho-FAK and total FAK in whole cell lysates from mM3L and FC1199B treated with recombinant SEMA3A. GAPDH was used as loading control in D and E. (F) Quantification of apoptotic cells from the anoikis assay of the SEMA3A knockout mM3L treated with vehicle, with the RhoK inhibitor (RKi), the recombinant SEMA3A (S3A-FC) or the combination of S3A-FC and defactinib (FAKi). Data are displayed as mean±SD of four technical replicates. *p<0.05, ***p<0.001 by Student's t-test. (G) Stacked bar plot displaying the percentage of mice (n=7 per group) displaying lung metastases on tail-vein injection of *Sema3a* proficient (NTC) and deficient (KO) cells. Scale bar 1 mm. GAPDH, glyceraldehyde 3-phosphate dehydrogenase; Poly-HEMA, poly(2-hydroxyethyl methacrylate).

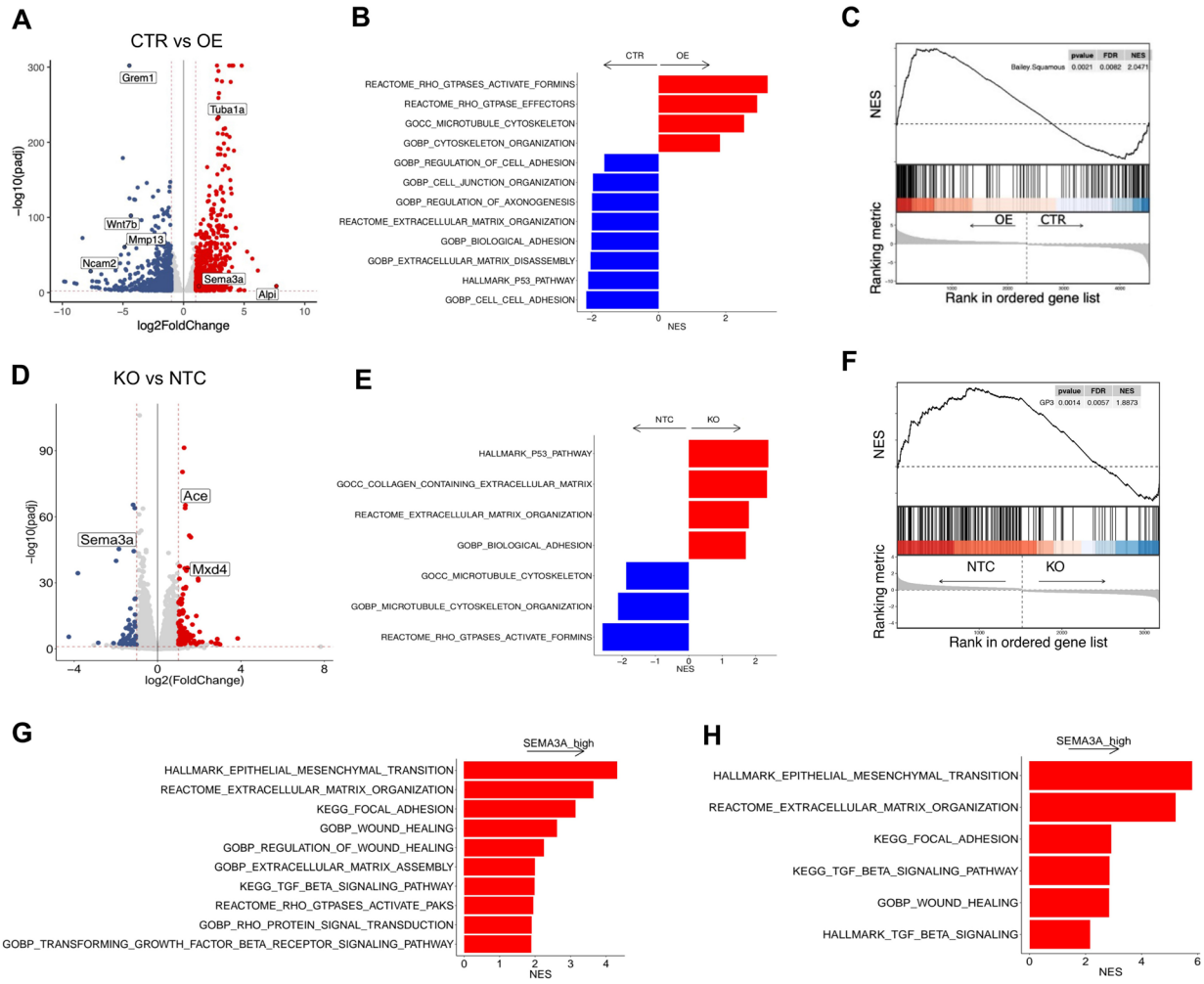

Figure 5 Transcriptomic changes following SEMA3A perturbation. (A) Volcano plot of the differences in gene expression between control (CTR, n=3) and *Sema3a* overexpression (OE n=3). Indicated are some of the genes with log2FC expression≥2 and adjusted p<0.05. See online supplemental table S1 for the full list of differentially expressed genes. (B) Enrichment of selected pathways (GSEA) when comparing FC1199B *Sema3a*^{low} (CTR) and FC1199B overexpressing *Sema3a* (OE). See also online supplemental table S2. (C) GSEA plot evaluating the Squamous signature[6] on *Sema3a* overexpression (OE) in FC1199B cells. (D) Volcano plot of the differences in gene expression between control (NTC, n=3) and *Sema3a* knockout (KO, n=3). Indicated are some of the genes with log2FC expression≥2 and adjusted p<0.05. See online supplemental table S3 for the full list of differentially expressed genes. (E) Enrichment of selected pathways (GSEA) when comparing *Sema3a* proficient (NTC) and deficient (KO) FC1199A cells. See also online supplemental table S4. (F) GSEA plots evaluating the Gene Programme 3 (GP3, TGFβ pathway)[6] on *Sema3a* knockout in FC1199A cells. (G–H) Enrichment of selected pathways when comparing SEMA3A high and low tissues from the ICGC[6] (G) and the PanCuRx[7] (H) cohorts. See also online supplemental tables S5–S8. In B, E, G and H, GSEA was performed using gene sets from Hallmark, GO, KEGG, Reactome and HP databases in MsigDB library. Displayed gene sets that passed false discovery rate <0.05. GSEA, gene set enrichment analysis.

Immunophenotyping showed that SEMA3A promoted abundant intratumoural infiltration of macrophages (F4/80+cells) while concurrently reducing intratumoural density of T cells (CD3+and CD8+ T cells) (figure 6E,F, online supplemental figure S6E). The in situ immunophenotypic results were confirmed by FACS analysis of whole-tumour tissues (online supplemental figure S6F), which further showed no significant SEMA3A-induced changes in other myeloid or T cell (eg, Treg) compartments. Finally, we analysed the transcriptomic data from the ICGC cohort dividing tissues based on the expression of *SEMA3A* (see the 'Methods' section). Consistent with our findings in the mouse models, transcriptional signatures of tumour-associated macrophages (TAMs) were significantly enriched in *SEMA3A* high tumours (online supplemental figure S6G). These results prompted us to investigate the role of tumour-derived SEMA3A on macrophage recruitment and polarisation.

Increased intratumoural infiltration of TAMs contributes to the aggressive behaviour of SEMA3A high tumours

To model the potential effect of SEMA3A on macrophages' recruitment, we used the transwell migration assay. The monocyte/macrophage cell line RAW 264.7 was first polarised towards M1-like or M2-like macrophages (online supplemental figure S7A, see the 'Methods' section). Then, polarised and non-polarised macrophages were seeded with Matrigel in transwell to perform an invasion assay. As expected, a medium containing 20% FBS supported the invasion in all macrophages' phenotypes (figure 7A). Similarly, recombinant SEMA3A promoted the invasion of all macrophages' phenotypes, although to a different extent (figure 7A). Silencing of the receptors (either *Nrp1* or *Plxna1*) completely abrogated the chemoattractive effects of SEMA3A (figure 7A).

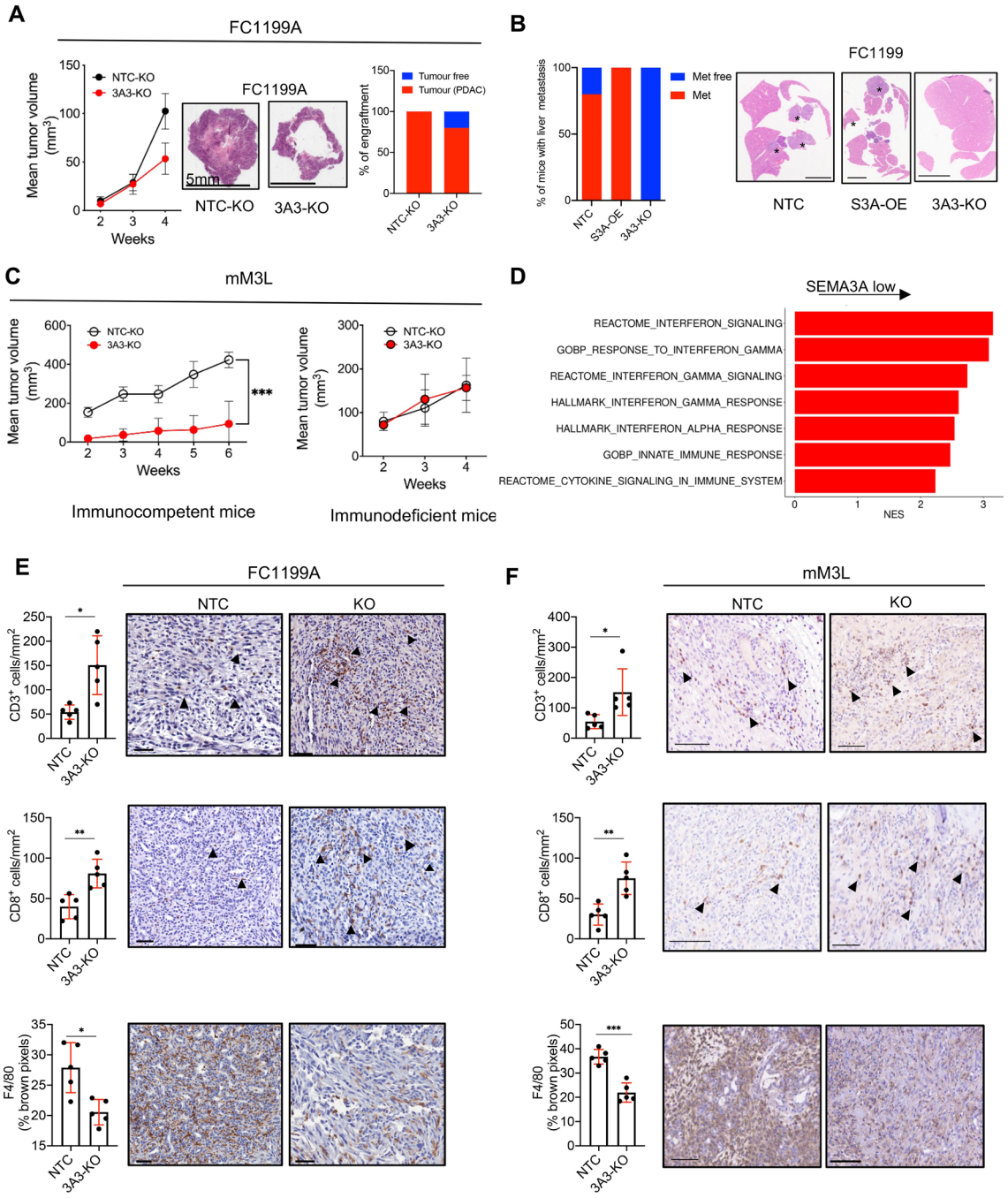

Figure 6 SEMA3A promotes growth of PDAC cells through modification of the tumour microenvironment. (A) On the left, line graph showing tumour volumes (mm^3) of pancreatic masses detected on the orthotopic injection of 1×10^5 cells from FC1199A (n=11/group). Means±SD are shown; difference not reaching statistical significance by Student's t-test. Middle panel, histological images of transplanted tumours; scale bar as indicated. On the right, stacked bar plot displaying the percentage of tumour bearing mice in the two cohorts (NTC and KO). (B) Stacked bar plot displaying the percentage of mice (n=5 per group) displaying liver metastases on intrasplenic injection of *Sema3a* proficient (NTC) deficient (KO) and overexpressing (OE) FC1199 cells. Scale bar 1 mm. (C) Line graph showing tumour volumes (mm^3) of pancreatic masses detected on injection of 1×10^6 cells from mM3L organoids into the pancreata of immunocompetent (n=10 mice per group, left panel) or immunodeficient (n=5 mice per group, right panel) mice. Means±SD are shown. ****p<0.001 by two-way ANOVA with Sidak's test for multiple comparison. Tumour volume was assessed using Vevo 2100 System with a MS250, 13–24 MHz scanhead (Visual Sonics). (D) Enrichment of selected pathways when comparing tissues from *Sema3a* deficient (n=3) and proficient (n=3) tumours. GSEA was performed using gene sets from Hallmark, GO, Reactome and HP databases in MsigDB library. Displayed gene sets that passed false discovery rate <0.05. See online supplemental tables S9 and S10 for details. (E–F) Representative immunohistochemical staining for T cells markers (CD3 and CD8) and the macrophage marker F4/80 in pancreatic tissues from mice transplanted with: (E) FC1199A cells or (F) mM3L organoid cultures stably transduced with either non-targeting vector (NTC) or gRNA targeting *Sema3a* (KO). Scale bars, 50 µm. Quantification is provided on the left as mean±SD (see the 'Methods' section). At least five individual areas per case and a minimum of five mice/arm were evaluated. Arrowheads indicate positive staining. ANOVA, analysis of variance.

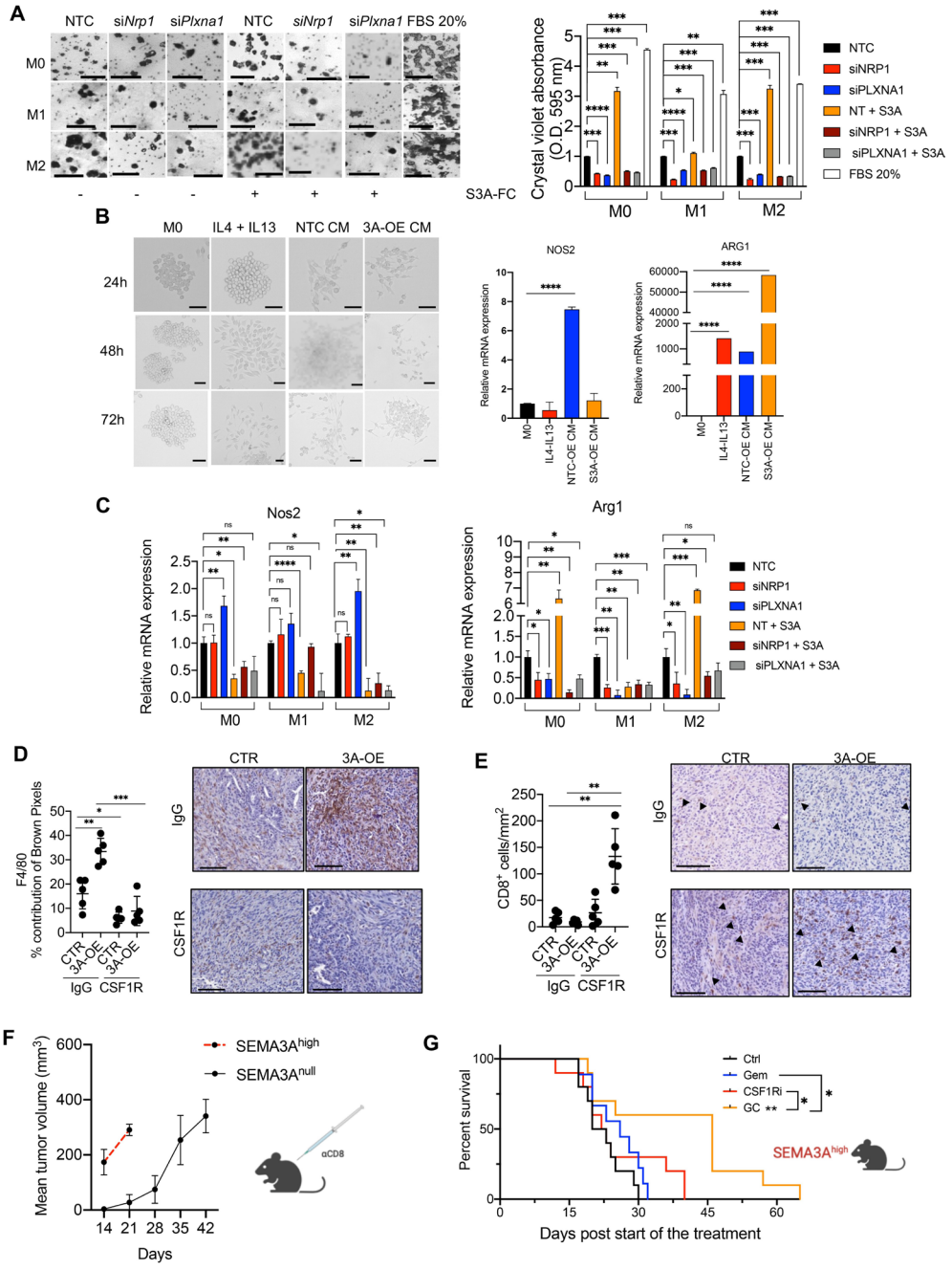

Figure 7 Increased intratumoural infiltration of TAMs contributes to the aggressive behaviour of SEMA3A high tumours. (A) Bright-field images of migrated macrophages in the transwell assay (see methods, left panel). The quantification is provided on the right as bar plots displaying mean±SD of the optical density values from three technical replicates. ***p<0.001, **p<0.01, *p<0.05 by unpaired Student's t-test. (B) Left panel, brightfield images of mouse RAW 264.7 cells treated as indicated for up to 72 hours. From left to right, untreated (M0), combination of IL4+IL13, conditioned media from control cells and conditioned media from cells overexpressing SEMA3A. Right panel, qPCR showing relative mRNA expression of *Nos2* and *Arg1*. Data are mean of three technical replicates. ****p<0.0001 by Student's t-test. (C) qPCR showing relative mRNA expression of *Nos2* (left) and *Arg1* (right). Data are mean of three technical replicates. ***p<0.001, **p<0.01, *p<0.05 by unpaired Student's t-test. (D) Representative immunohistochemical staining for the macrophage marker F4/80 in pancreatic tissues from mice transplanted with FC1199B cells stably transduced with either mock (CTR) or a vector carrying *Sema3a* ORF (3A-OE) treated with control IgG or CSF1R monoclonal antibody. (E) Representative immunohistochemical staining for the cytotoxic T cell marker (CD8) in pancreatic tissues from mice transplanted with FC1199B cells stably transduced with either mock (CTR) or a vector carrying *Sema3a* ORF (3A-OE) treated with control IgG or CSF1R monoclonal antibody. In E and F, scale bars, 50 µm. Quantification is provided on the left as mean±SD (see the 'Methods' section). At least five individual areas per case and a minimum of five mice/arm were evaluated. Arrowheads indicate positive staining. (F) Line graph showing tumour volumes (mm^3) of pancreatic masses detected in mice transplanted with SEMA3A overexpressing (SEMA3Ahigh) or null (SEMA3Anull) cells treated with αCD8 (CD8, n=10). (G) Kaplan-Meier survival analysis of mice transplanted with SEMA3A high cells and treated with control IgG (Ctrl, n=10), Gemcitabine (Gem, n=10), αCSF1R (CSF1Ri, n=10) or combination of Gemcitabine and αCSF1R (GC, n=10). Statistical differences identified by log-rank test.

Next, we evaluated the effect of SEMA3A on the polarisation of macrophages using both RAW 264.7 and bone-marrow-derived monocytes. We grew RAW 264.7 in standard medium, in medium containing a cocktail of cytokine inducing the M2-like state (IL4 and IL13), and in conditioned media from SEMA3A proficient and deficient cells. As expected, the combined treatment with IL4 and IL13 induced morphological and molecular activation (figure 7B) of the macrophages, with increased expression of *Arg1* (marker of M2-like macrophages) and a slight (although not significant) reduction of the expression of the M1-like gene *Nos2*. As opposed to the conditioned medium from *Sema3a* deficient cells, the conditioned medium from SEMA3A expressing tumour cells significantly induced *Arg1* expression without eliciting *Nos2* expression. Coherently, the treatment of bone-marrow-derived monocytes with recombinant SEMA3A induced protein and mRNA expression of M2-like markers (online supplemental figure S7B,C). We then evaluated the effect of receptor knockdown on the polarising effect of SEMA3A. In unperturbed conditions, SEMA3A treatment reduced *Nos2* expression in all macrophages' subsets, while inducing *Arg1* expression in M0, M2 but not M1 (figure 7C). Following silencing of the receptors, SEMA3A induced changes in *Nos2* and *Arg1* expression were prevented in all subsets (figure 7C). The in vitro data were consistent with the higher density of CD206+macrophages in tumour tissues from SEMA3A expressing cells as evidenced by both FACS analysis (online supplemental figure S6F) and immunophenotyping (online supplemental figure S7D)

To understand whether the reduced T cells infiltration of SEMA3A^{high} tumours was due, at least in part, to the abundance of TAM at the tumour bed, we targeted macrophages using a monoclonal antibody against CSF1R (αCSF1R). As shown in online supplemental figure S7E, immunocompetent mice were treated daily with αCSF1R 3 days prior the transplantation with SEMA3A proficient and deficient cells along with the control. The treatment with αCSF1R continued every other day until endpoint and tumour growth monitored by manual palpation and ultrasound imaging. At endpoint, we observed a significant reduction of intratumoural infiltration by macrophages (F4/80+cells) in tumours from mice treated with αCSF1R regardless of the SEMA3A status (figure 7D). Cytometric analyses of blood samples from tumour-bearing mice also confirmed the reduction of F4/80+cells with no significant effect on Ly6C$^+$Ly6G$^+$ or Ly6C$^+$ cells (online supplemental figure S7F), which is in line with the inhibition of CSF1R in mouse PDAC using a small molecule.[10] Only in tumours established by SEMA3A overexpressing cells, the depletion of macrophages was associated with increased intratumoural infiltration by CD8+T cells (figure 7E).

Given the prominent difference in T cell infiltration following macrophages depletion, we sought to explore whether CD8+T cell depletion would have a different effect on the growth of SEMA3A^{high} and SEMA3A^{low} tumours. The depletion of CD8+T cells led to the rapid progression of the disease of SEMA3A^{high} so that mice succumbed to the disease within 7 days from the beginning of the treatment (figure 7F). This result suggested that CD8+T cells play a dominant role in controlling the disease in the setting of SEMA3A+tumours. Next, we tried to assess whether depletion of macrophages had differential effect on the disease control achievable through pharmacological treatment. First, we tested the effect of CSF1R inhibition alone or in combination with gemcitabine on the survival of mice bearing tumours from either *Sema3a* high or low cells (online supplemental figure S7G). In line with their less aggressive behaviour, SEMA3A low tumours responded to all the treatments, yet gemcitabine monotherapy did not reach statistical significance (p=0.08) (online supplemental figure S7H). SEMA3A high tumours responded poorly to both gemcitabine and CSF1R inhibition as monotherapy, and only the combination significantly extended the survival of the mice (figure 7G). On depletion of CD8+T cells, the combination lost its antitumour activity in *Sema3a* expressing tumours (online supplemental figure S7I), thereby suggesting that its efficacy was at least in part mediated by the increased infiltration of T cells.

DISCUSSION

Genome-wide analyses of PDAC tissues have evidenced the dysregulation of the axon guidance pathway in this dismal disease.[14 16 55 56] Here, we investigated the role of the diffusible axon guidance cue SEMA3A, whose tissue expression has been previously linked to poor clinical outcomes in PDAC.[14 15] We showed that SEMA3A is highly expressed by neoplastic cells with squamous differentiation and a basal-like phenotype. Of the two PDAC epithelial cell lineages,[6–9] the basal-like/squamous phenotype displays a more aggressive behaviour and it is enriched in post-treatment tumours as well as in metastases.[7] We found that both cell-intrinsic (eg, biallelic inactivation of p53) and cell extrinsic (eg, TGF-β1) factors promoting the basal-like/squamous subtype induce expression of SEMA3A in PDAC cells. Mechanistically, we demonstrated that SEMA3A exerts both cell-autonomous and non-cell autonomous effects to support the progression of PDAC. Cell-intrinsically, SEMA3A contributes to define a mesenchymal-like phenotype, including enhanced migratory capability. Moreover, tumour-derived SEMA3A activates FAK through the canonical SEMA3A-NRP1 axis to promote anoikis resistance. In keeping with that, SEMA3A overexpressing mouse PDAC cells display superior metastatic competence compared with cells lacking SEMA3A. Moreover, SEMA3A expressing cells induces protumourigenic changes in the TME with increased density of macrophages and significantly reduced infiltration of T cells.

TAMs are the most abundant leucocyte population in the stroma of both mouse and human PDAC[10] and they contribute to establish an 'immunologically cold' microenvironment also through T cell exclusion.[57] Specifically, in the context of SEMA3A expressing tumours, the depletion of macrophages led to increased intratumoural infiltration of T cells and the maximisation of therapeutic benefit from gemcitabine. The axon guidance is a highly conserved pathway involved in the proper formation of neural circuits during the development of the central nervous system (CNS).[52] The axon guidance genes include membrane-bound or diffusible ligands (Netrins, Semaphorins, Ephrins, Slits) that act either as chemoattractant or chemorepellent for growing axons and migrating neurons. These axon guidance cues and their receptors are also expressed outside of the CNS where they regulate cell-to-cell, cell-to-extracellular matrix interactions and tissue morphogenesis.[58] At the molecular level, all guidance cues influence cell motility through the engagement of the Rac family of small GTPases.[58]

Here, we found that SEMA3A sustains gene programmes related to EMT and increases FAK signalling in mouse PDAC cells. The activation of those molecular pathways parallels a functional phenotype of mesenchymal-like cells with migratory capability and increased metastatic competence. Most of the previous studies in PDAC have focused on investigating the role of members of the Slit/Robo axis on the PDAC malignant traits of PDAC as well as its cell identity.[17 19–22] Of the four classes of ligands, semaphorins represent the largest family and were originally identified as chemorepellent proteins in the nervous system.[23 24] SEMA3A belongs to the class 3 of secreted semaphorins and its potential role in cancer still needs to be elucidated. Indeed, several works have proposed a tumour suppressive role for SEMA3A, which has been reported to restrain tumour growth by hampering tumour angiogenesis.[59] In PDAC, an NRP1-independent superagonist SEMA3A was used as vasculature normalising agent which demonstrated antitumour activity.[60] Moreover, there are contradictory results on the effect of SEMA3A on recruitment and activation of TAMs. TAMs have an established protumoural function and shares features with M2-like macrophages, including the expression of Arginase 1 and of the Mannose Receptor CD206.[61 62] Carrer *et al* reported that SEMA3A recruits a subset of resident Nrp1+antitumoural macrophages,[63] while Casazza *et al* found that SEMA3A entraps protumoural macrophages in highly hypoxic areas.[64] Finally, Wallerius *et al* reported a differential effect of SEMA3A on the proliferation of M2 and M1-like macrophages[65]: SEMA3A favoured the expansion of antitumoural M1-like macrophages which was associated with the recruitment of cytotoxic T cells and a tumour-inhibiting effect.

In our preclinical models, tumour cells derived SEMA3A contributed to define an immunosuppressive TME with abundant macrophages and reduced density of CD8+T cells. Our findings perfectly align with the elevated expression of *SEMA3A* in basal-like/squamous PDAC, which are characterised by elevated infiltration of TAM and scant T cells.[10] In vitro, SEMA3A functioned as chemoattractant for different macrophages subsets and further skewed the macrophage population towards an M2-like phenotype. Accordingly, the depletion of macrophages with the monoclonal antibody against CSF1R favoured intratumoural infiltration of cytotoxic T cells specifically in the context of SEMA3A^{high} tumours. Nonetheless, we cannot exclude that the establishment of an immunosuppressive microenvironmental contexture in SEMA3A^{high} tumours is also contributed by stromal-derived SEMA3A as well as by SEMA3A-induced neural plasticity.[66] Furthermore, we found that SEMA3A^{high} tumours were more resistant to gemcitabine treatment than the SEMA3A^{low} tumours, which perfectly aligns with the more aggressive biological behaviour of SEMA3A^{high} tumours. However, the depletion of macrophages resulted in a significant greater benefit in terms of overall survival following chemotherapy for tumours with high expression of SEMA3A.

Overall, we show here that SEMA3A is a functional marker of aggressive PDAC that promotes tumour progression through modification of the local microenvironment and by enhancing the metastatic competence of neoplastic cells. However, a greater infiltration of CD8+T cells is observed in SEMA3A^{high} tumours on macrophages depletion, suggesting a potential chemoattractant role of SEMA3A for T cells. While this aspect needs further elucidation, we have provided proof that the disease control in the setting of SEMA3A^{high} tumours is critically dependent on CD8+T cells. In conclusion, we show that *SEMA3A* is a stress-sensitive locus that enhances the malignant phenotype of PDAC cells through both cell-intrinsic and cell-extrinsic mechanisms.

Author affiliations
[1]Department of Engineering for Innovation Medicine, University of Verona, Verona, Italy
[2]Department of Medicine, University of Verona, Verona, Italy
[3]ARC-Net Research Centre, University of Verona, Verona, Italy
[4]Department of Diagnostic and Public Health, University of Verona, Verona, Italy
[5]Division of Immunology, Transplantation and Infectious Diseases, IRCSS San Raffaele, Milan, Italy
[6]Human Technopole, Milan, Italy
[7]Department of Biochemistry and Molecular Biology, University of Würzburg, Wurzburg, Germany
[8]Department of Medical and Surgical Sciences, Fondazione Policlinico Universitario Agostino Gemelli IRCCS, Roma, Italy
[9]Microbiology and Molecular Genetics, UC Davis Department of Microbiology, Davis, California, USA
[10]Division of Systems Toxicology, Department of Biology, University of Konstanz, Konstanz, Germany
[11]Wolfson Wohl Cancer Research Centre, University of Glasgow, Glasgow, UK
[12]Cold Spring Harbor Laboratory, Cold Spring Harbor, New York, USA

X Michele Bevere @michele_bevere, Silvia Andreani @SilviaAndreani7, Francesco De Sanctis @FrancescoDS82, Chang-il Hwang @ChangilHwang and Stefano Ugel @StefanoUgel

Acknowledgements We gratefully acknowledge the Centro Piattaforme Tecnologiche (CPT—University of Verona, Verona, Italy) for granting access to the genomic facility of the University of Verona. Additionally, we are grateful to Sonia Grimaldi, Nicola Sperandio, and Giada Bonizzato (ARC-Net Research Centre, University of Verona) for the assistance provided with the generation of organoid models. We also thank Professor Valeria Barresi, from the Department of Diagnostics and Public Health, for her help in the interpretation of the results. Some of the illustrations have been created with Biorender.com.

Contributors FL, SU and VC conceived and designed the research; FL and VC developed the idea; FL, EF and MB performed animal experiments; FL and LV performed experiments with organoids; FL and C-iH performed in vitro experiments; AA, CF, TW and FDS performed cytofluorimetric analysis; FL, AA and CF performed experiments with monocytes and macrophages; FL and AM performed ISH experiments; PD, PB, FP and DP analysed omics data and generated displays; DP analysed single cell sequencing data; SD'a and SA established human organoids cultures; RTL, CC and GP collected tissue samples. FL, EF and LV performed histology and immunohistochemistry of all human and mouse tissue samples. AS, FL and VC analysed the human tissues; IA assisted with the design of Chip-qPCR experiments and the interpretation of the data; FL, SU, FDS and VC analysed data relative to the mouse TME; DT provided human and mouse models; SU and VC designed the in vivo treatment experiments; FL, SU and VC interpreted the data; FL, FP, DP and VC wrote the manuscript. VC supervised the study and act as guarantor.

Funding VC is supported by Associazione Italiana Ricerca sul Cancro (AIRC; grant no. 18178; 28801). VC is also supported by the EU (MSCA project PRECODE, grant No: 861196), the National Cancer Institute (NCI, HHSN26100008) and Fondazione Nadia Valsecchi Onlus. AS is supported by AIRC (26343); EF was supported by AIRC (25286;29692). LV was supported by AIRC (29528). PD has been supported by Fondazione Nadia Valsecchi Onlus and Fondazione Umberto Veronesi. MB is supported by AIRC fellowship for Italy (28054) and Fondazione Nadia Valsecchi Onlus. GP is supported by AIRC (MFAG AIRC; grant no. 29224). CC is supported by AIRC (MFAG AIRC Grant 'Luigi Bonatti e Anna Maria Bonatti Rocca'; grant no. 23681). This study was conducted with the support of the Ontario Institute for Cancer Research through funding provided by the Government of Ontario. This work has been supported by the DFG under the TRR353/1 "Death Decision" project A05 to IA.

Competing interests None declared.

Patient and public involvement Patients and/or the public were not involved in the design, or conduct, or reporting, or dissemination plans of this research.

Patient consent for publication Consent obtained directly from patient(s).

Ethics approval This study involves human participants and was approved by Comitato Etico Azienda Ospedaliera Universitaria Integrata, Prot. 52070, Prog. 1885 on 17 November 2010. Participants gave informed consent to participate in the study before taking part.

Provenance and peer review Not commissioned; externally peer reviewed.

Data availability statement All data relevant to the study are included in the article or uploaded as online supplemental information. Data will be made available following acceptance.

ORCID iDs
Silvia Andreani http://orcid.org/0000-0002-3715-1553
Chang-il Hwang http://orcid.org/0000-0002-5710-7672
Carmine Carbone http://orcid.org/0000-0001-5168-747X
Vincenzo Bronte http://orcid.org/0000-0002-3741-5141
David Tuveson http://orcid.org/0000-0002-8017-2712
Aldo Scarpa http://orcid.org/0000-0003-1678-739X
Vincenzo Corbo http://orcid.org/0000-0002-6340-8009

REFERENCES

1 Rahib L, Wehner MR, Matrisian LM, *et al*. Estimated projection of US cancer incidence and death to 2040. *JAMA Netw Open* 2021;4:e214708.
2 Casolino R, Braconi C, Malleo G, *et al*. Reshaping preoperative treatment of pancreatic cancer in the era of precision medicine. *Ann Oncol* 2021;32:183–96.
3 Barreto SG, Pandanaboyana S, Ironside N, *et al*. Does revision of resection margins based on frozen section improve overall survival following pancreatoduodenectomy for pancreatic ductal adenocarcinoma? A meta-analysis. *HPB (Oxford)* 2017;19:573–9.
4 Tanaka M, Mihaljevic AL, Probst P, *et al*. Meta-analysis of recurrence pattern after resection for pancreatic cancer. *Br J Surg* 2019;106:1590–601.
5 Tummers WS, Groen JV, Sibinga Mulder BG, *et al*. Impact of resection margin status on recurrence and survival in pancreatic cancer surgery. *Br J Surg* 2019;106:1055–65.
6 Bailey P, Chang DK, Nones K, *et al*. Genomic analyses identify molecular subtypes of pancreatic cancer. *Nature* 2016;531:47–52.
7 Chan-Seng-Yue M, Kim JC, Wilson GW, *et al*. Transcription phenotypes of pancreatic cancer are driven by genomic events during tumor evolution. *Nat Genet* 2020;52:231–40.
8 Collisson EA, Sadanandam A, Olson P, *et al*. Subtypes of pancreatic ductal adenocarcinoma and their differing responses to therapy. *Nat Med* 2011;17:500–3.
9 Moffitt RA, Marayati R, Flate EL, *et al*. Virtual microdissection identifies distinct Tumor- and stroma-specific subtypes of pancreatic ductal adenocarcinoma. *Nat Genet* 2015;47:1168–78.
10 Candido JB, Morton JP, Bailey P, *et al*. Csf1R(+) Macrophages sustain pancreatic tumor growth through T cell suppression and maintenance of key gene programs that define the squamous subtype. *Cell Rep* 2018;23:1448–60.
11 Raghavan S, Winter PS, Navia AW, *et al*. Microenvironment drives cell state, plasticity, and drug response in pancreatic cancer. *Cell* 2021;184:6119–37.
12 Hwang WL, Jagadeesh KA, Guo JA, *et al*. Single-nucleus and spatial transcriptome profiling of Pancreatic cancer identifies multicellular dynamics associated with neoadjuvant treatment. *Nat Genet* 2022;54:1178–91.
13 Grünwald BT, Devisme A, Andrieux G, *et al*. Spatially confined sub-tumor microenvironments in pancreatic cancer. *Cell* 2021;184:5577–92.
14 Biankin AV, Waddell N, Kassahn KS, *et al*. Pancreatic cancer genomes reveal aberrations in axon guidance pathway genes. *Nature* 2012;491:399–405.
15 Müller MW, Giese NA, Swiercz JM, *et al*. Association of axon guidance factor semaphorin 3A with poor outcome in pancreatic cancer. *Int J Cancer* 2007;121:2421–33.
16 Nones K, Waddell N, Song S, *et al*. Genome-wide DNA methylation patterns in pancreatic ductal adenocarcinoma reveal epigenetic deregulation of SLIT-ROBO, Itga2 and MET signaling. *Int J Cancer* 2014;135:1110–8.
17 Krebs N, Klein L, Wegwitz F, *et al*. Axon guidance receptor Robo3 modulates subtype identity and prognosis via AXL-associated inflammatory network in pancreatic cancer. *JCI Insight* 2022;7:e154475.
18 Di Chiaro P, Nacci L, Brandini S, *et al*. Coexisting Morpho-Biotypes unveil the regulatory bases of phenotypic plasticity in pancreatic ductal adenocarcinoma. *Cancer Biology* [Preprint].
19 Escot S, Willnow D, Naumann H, *et al*. Robo signalling controls pancreatic progenitor identity by regulating Tead transcription factors. *Nat Commun* 2018;9:5082.
20 Göhrig A, Detjen KM, Hilfenhaus G, *et al*. Axon guidance factor SLIT2 inhibits neural invasion and metastasis in pancreatic cancer. *Cancer Res* 2014;74:1529–40.
21 Pinho AV, Van Bulck M, Chantrill L, *et al*. Robo2 is a stroma suppressor gene in the pancreas and acts via TGF-beta signalling. *Nat Commun* 2018;9:5083.
22 Secq V, Leca J, Bressy C, *et al*. Stromal SLIT2 impacts on pancreatic cancer-associated neural remodeling. *Cell Death Dis* 2015;6:e1592.
23 Kolodkin AL, Matthes DJ, O'Connor TP, *et al*. Fasciclin IV: sequence, expression, and function during growth cone guidance in the grasshopper embryo. *Neuron* 1992;9:831–45.
24 Kong Y, Janssen BJC, Malinauskas T, *et al*. Structural basis for Plexin activation and regulation. *Neuron* 2016;91:548–60.
25 Cancer Genome Atlas Research Network. Electronic address: andrew_aguirre@dfci.harvard.edu, Cancer Genome Atlas Research Network. Integrated genomic characterization of pancreatic ductal adenocarcinoma. *Cancer Cell* 2017;32:185–203.
26 Hingorani SR, Petricoin EF III, Maitra A, *et al*. Preinvasive and invasive ductal pancreatic cancer and its early detection in the mouse. *Cancer Cell* 2003;4:437–50.
27 Hingorani SR, Wang L, Multani AS, *et al*. Trp53R172H and KrasG12D cooperate to promote chromosomal instability and widely metastatic Pancreatic Ductal adenocarcinoma in mice. *Cancer Cell* 2005;7:469–83.
28 Filippini D, Agosto SD, Delfino P, *et al*. Immunoevolution of mouse pancreatic organoid isografts from preinvasive to metastatic disease. *Sci Rep* 2019;9:12286.
29 Boj SF, Hwang C-I, Baker LA, *et al*. Organoid models of human and mouse ductal pancreatic cancer. *Cell* 2015;160:324–38.
30 Baslan T, Morris JP 4th, Zhao Z, *et al*. Ordered and deterministic cancer genome evolution after P53 loss. *Nature* 2022;608:795–802.
31 Oni TE, Biffi G, Baker LA, *et al*. Soat1 promotes Mevalonate pathway dependency in pancreatic cancer. *J Exp Med* 2020;217:e20192389.
32 Morris JP IV, Yashinskie JJ, Koche R, *et al*. Alpha-Ketoglutarate links P53 to cell fate during tumour suppression. *Nature* 2019;573:595–9.
33 DeNicola GM, Karreth FA, Humpton TJ, *et al*. Oncogene-induced NRF2 transcription promotes ROS detoxification and tumorigenesis. *Nature* 2011;475:106–9.
34 Zhang D, Lindstrom A, Kim EJ, *et al*. SEMA3C supports pancreatic cancer progression by regulating the autophagy process and tumor immune Microenvironment. *Front Oncol* 2022;12:890154.
35 Grün D, Muraro MJ, Boisset J-C, *et al*. De Novo prediction of stem cell identity using single-cell transcriptome data. *Cell Stem Cell* 2016;19:266–77.
36 Lawlor N, George J, Bolisetty M, *et al*. Single-cell transcriptomes identify human islet cell signatures and reveal cell-type-specific expression changes in type 2 diabetes. *Genome Res* 2017;27:208–22.
37 Muraro MJ, Dharmadhikari G, Grün D, *et al*. A single-cell transcriptome atlas of the human pancreas. *Cell Syst* 2016;3:385–94.
38 Segerstolpe Å, Palasantza A, Eliasson P, *et al*. Single-cell transcriptome profiling of human pancreatic islets in health and type 2 diabetes. *Cell Metab* 2016;24:593–607.
39 Tang Z, Li C, Kang B, *et al*. GEPIA: a web server for cancer and normal gene expression profiling and interactive analyses. *Nucleic Acids Res* 2017;45:W98–102.
40 Lin W, Noel P, Borazanci EH, *et al*. Single-cell Transcriptome analysis of tumor and stromal compartments of pancreatic ductal adenocarcinoma primary tumors and metastatic lesions. *Genome Med* 2020;12:80.
41 Peng J, Sun B-F, Chen C-Y, *et al*. Single-cell RNA-Seq highlights intra-Tumoral heterogeneity and malignant progression in Pancreatic Ductal adenocarcinoma. *Cell Res* 2019;29:725–38.
42 Steele NG, Carpenter ES, Kemp SB, *et al*. Multimodal mapping of the tumor and peripheral blood immune landscape in human Pancreatic cancer. *Nat Cancer* 2020;1:1097–112.
43 Korsunsky I, Millard N, Fan J, *et al*. Fast, sensitive and accurate integration of single-cell data with harmony. *Nat Methods* 2019;16:1289–96.
44 Aran D, Looney AP, Liu L, *et al*. Reference-based analysis of lung single-cell sequencing reveals a transitional Profibrotic macrophage. *Nat Immunol* 2019;20:163–72.
45 Gao R, Bai S, Henderson YC, *et al*. Delineating copy number and Clonal substructure in human tumors from single-cell Transcriptomes. *Nat Biotechnol* 2021;39:599–608.
46 Franzén O, Gan L-M, Björkegren JLM. Panglaodb: a web server for exploration of Mouse and human single-cell RNA sequencing data. *Database (Oxford)* 2019;2019:baz046.
47 Elyada E, Bolisetty M, Laise P, *et al*. Cross-species single-cell analysis of Pancreatic Ductal adenocarcinoma reveals antigen-presenting cancer-associated fibroblasts. *Cancer Discov* 2019;9:1102–23.
48 Frisch SM, Vuori K, Ruoslahti E, *et al*. Control of adhesion-dependent cell survival by focal adhesion kinase. *J Cell Biol* 1996;134:793–9.
49 Paoli P, Giannoni E, Chiarugi P. Anoikis molecular pathways and its role in cancer progression. *Biochim Biophys Acta* 2013;1833:3481–98.
50 Lan L, Evan T, Li H, *et al*. Grem1 is required to maintain cellular heterogeneity in pancreatic cancer. *Nature* 2022;607:163–8.
51 Subramanian A, Tamayo P, Mootha VK, *et al*. Gene set enrichment analysis: a knowledge-based approach for interpreting genome-wide expression profiles. *Proc Natl Acad Sci U S A* 2005;102:15545–50.
52 Dickson BJ. Molecular mechanisms of axon guidance. *Science* 2002;298:1959–64.

53 Roe J-S, Hwang C-I, Somerville TDD, *et al*. Enhancer reprogramming promotes pancreatic cancer metastasis. *Cell* 2017;170:875–88.
54 D'Agosto S, Lupo F, Corbo V. Generation of pancreatic organoid-derived Isografts. *STAR Protoc* 2020;1:100047.
55 Corbo V, Ritelli R, Barbi S, *et al*. Mutational profiling of kinases in human tumours of pancreatic origin identifies candidate cancer genes in ductal and ampulla of vater carcinomas. *PLoS One* 2010;5:e12653.
56 Feigin ME, Garvin T, Bailey P, *et al*. Recurrent noncoding regulatory mutations in pancreatic ductal adenocarcinoma. *Nat Genet* 2017;49:825–33.
57 Beatty GL, Winograd R, Evans RA, *et al*. Exclusion of T cells from pancreatic carcinomas in mice is regulated by Ly6C(Low) F4/80(+) extratumoral macrophages. *Gastroenterology* 2015;149:201–10.
58 Hinck L. "The versatile roles of "axon guidance" cues in tissue morphogenesis". *Dev Cell* 2004;7:783–93.
59 Bussolino F, Giraudo E, Serini G. Class 3 Semaphorin in angiogenesis and lymphangiogenesis. *Chem Immunol Allergy* 2014;99:71–88.
60 Gioelli N, Maione F, Camillo C, *et al*. A rationally designed NRP1-independent Superagonist SEMA3A mutant is an effective anticancer agent. *Sci Transl Med* 2018;10:eaah4807.
61 Allavena P, Chieppa M, Bianchi G, *et al*. Engagement of the mannose receptor by tumoral mucins activates an immune suppressive phenotype in human tumor-associated macrophages. *Clin Dev Immunol* 2010;2010:547179.
62 Loke P, Nair MG, Parkinson J, *et al*. IL-4 dependent alternatively-activated macrophages have a distinctive in vivo gene expression phenotype. *BMC Immunol* 2002;3:7.
63 Carrer A, Moimas S, Zacchigna S, *et al*. Neuropilin-1 identifies a subset of bone marrow Gr1- monocytes that can induce tumor vessel normalization and inhibit tumor growth. *Cancer Res* 2012;72:6371–81.
64 Casazza A, Laoui D, Wenes M, *et al*. Impeding macrophage entry into hypoxic tumor areas by SEMA3A/NRP1 signaling blockade inhibits angiogenesis and restores antitumor immunity. *Cancer Cell* 2013;24:695–709.
65 Wallerius M, Wallmann T, Bartish M, *et al*. Guidance molecule SEMA3A restricts tumor growth by differentially regulating the proliferation of tumor-associated macrophages. *Cancer Res* 2016;76:3166–78.
66 Hung Y-H, Hou Y-C, Hsu S-H, *et al*. Pancreatic cancer cell-derived Semaphorin 3A promotes neuron recruitment to accelerate tumor growth and dissemination. *Am J Cancer Res* 2023;13:3417–32.

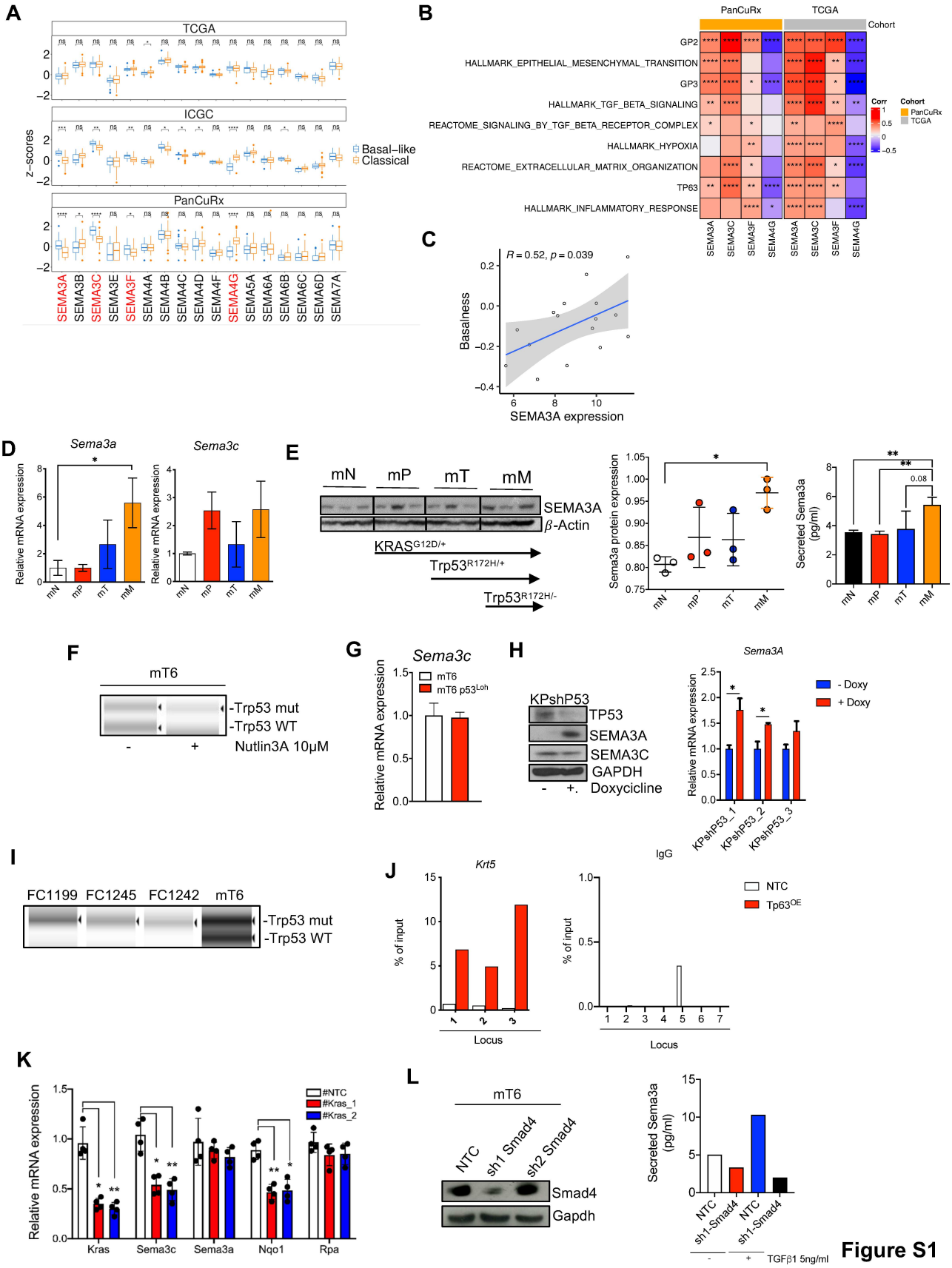
A
TCGA
ICGC
PanCuRx
z-scores
Basal–like
Classical
SEMA3A SEMA3B SEMA3C SEMA3E SEMA3F SEMA4A SEMA4B SEMA4C SEMA4D SEMA4F SEMA4G SEMA5A SEMA6A SEMA6B SEMA6C SEMA6D SEMA7A
B
PanCuRx
TCGA
Cohort
GP2
HALLMARK_EPITHELIAL_MESENCHYMAL_TRANSITION
GP3
HALLMARK_TGF_BETA_SIGNALING
REACTOME_SIGNALING_BY_TGF_BETA_RECEPTOR_COMPLEX
HALLMARK_HYPOXIA
REACTOME_EXTRACELLULAR_MATRIX_ORGANIZATION
TP63
HALLMARK_INFLAMMATORY_RESPONSE
SEMA3A SEMA3C SEMA3F SEMA4G
Corr
Cohort
PanCuRx
TCGA
C
R = 0.52, p = 0.039
Basalness
SEMA3A expression
D
Sema3a
Sema3c
Relative mRNA expression
mN mP mT mM
E
mN mP mT mM
SEMA3A
β-Actin
KRASG12D/+
Trp53R172H/+
Trp53R172H/-
Sema3a protein expression
Secreted Sema3a (pg/ml)
0.08
F
mT6
-Trp53 mut
-Trp53 WT
- +
Nutlin3A 10μM
G
Sema3c
mT6
mT6 p53Loh
Relative mRNA expression
H
KPshP53
TP53
SEMA3A
SEMA3C
GAPDH
- +. Doxycicline
Sema3A
- Doxy
+ Doxy
Relative mRNA expression
KPshP53_1
KPshP53_2
KPshP53_3
IgG
I
FC1199 FC1245 FC1242 mT6
-Trp53 mut
-Trp53 WT
J
Krt5
% of input
Locus
NTC
Tp63OE
K
Relative mRNA expression
#NTC
#Kras_1
#Kras_2
Kras Sema3c Sema3a Nqo1 Rpa
L
mT6
NTC sh1 Smad4 sh2 Smad4
Smad4
Gapdh
Secreted Sema3a (pg/ml)
NTC sh1-Smad4 NTC sh1-Smad4
- + TGFβ1 5ng/ml

Figure S1

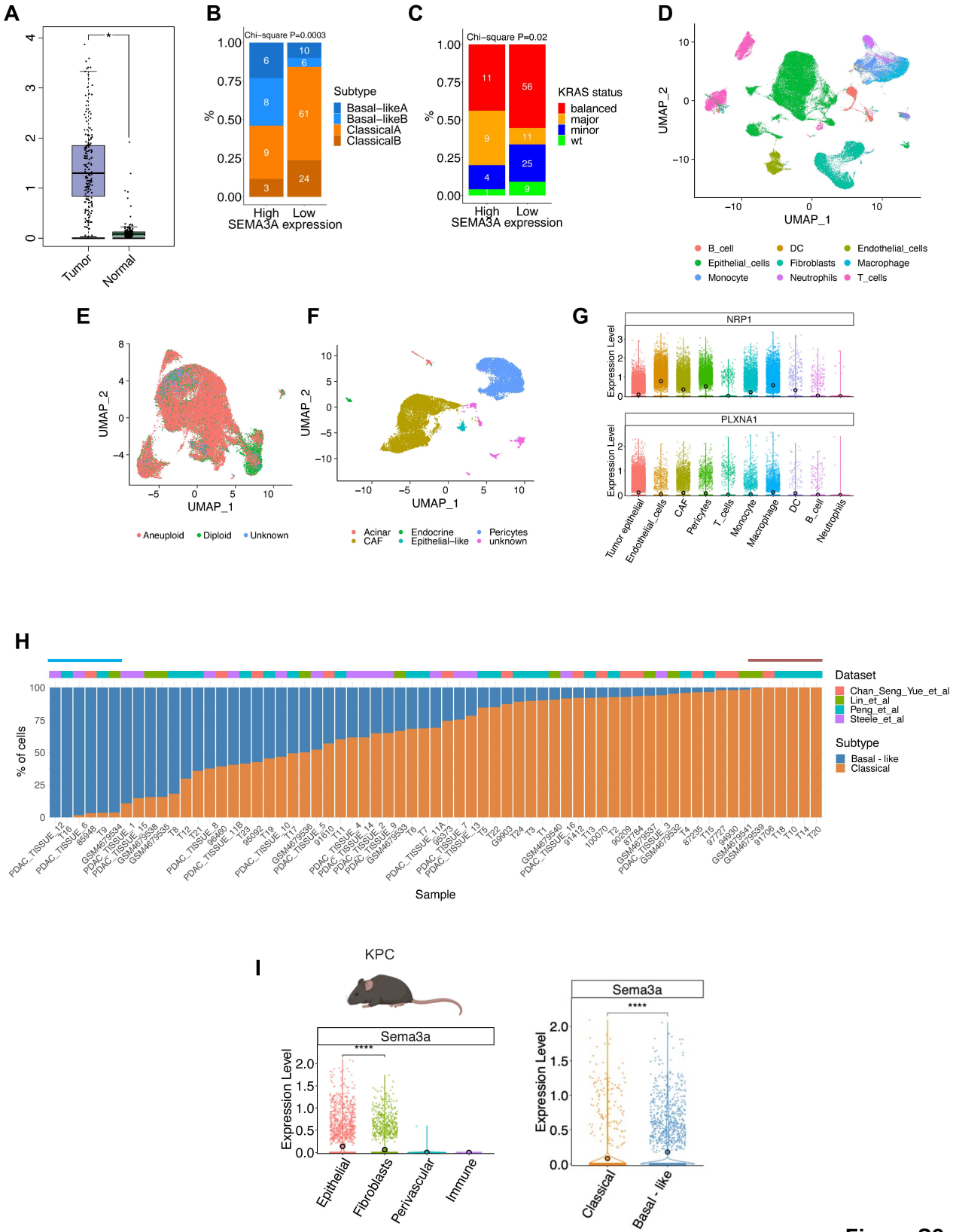
A
Tumor
Normal
B
Chi−square P=0.0003
Subtype
Basal−likeA
Basal−likeB
ClassicalA
ClassicalB
High
Low
SEMA3A expression
C
Chi−square P=0.02
KRAS status
balanced
major
minor
wt
D
UMAP_1
UMAP_2
B_cell
DC
Endothelial_cells
Epithelial_cells
Fibroblasts
Macrophage
Monocyte
Neutrophils
T_cells
E
Aneuploid
Diploid
Unknown
F
Acinar
CAF
Endocrine
Epithelial−like
Pericytes
unknown
G
NRP1
PLXNA1
Expression Level
Tumor epithelial
Endothelial_cells
CAF
Pericytes
T_cells
Monocyte
Macrophage
DC
B_cell
Neutrophils
H
% of cells
Sample
Dataset
Chan_Seng_Yue_et_al
Lin_et_al
Peng_et_al
Steele_et_al
Subtype
Basal - like
Classical
I
KPC
Sema3a
Expression Level
Epithelial
Fibroblasts
Perivascular
Immune
Classical
Basal - like

Figure S2

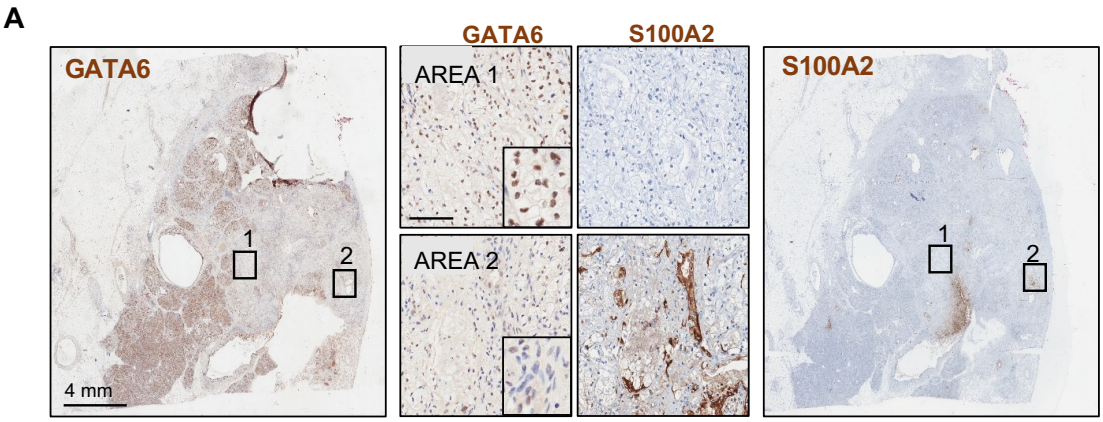

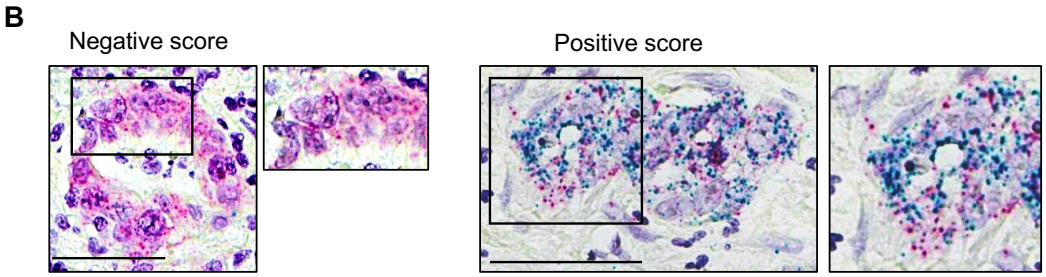

Staining score	Microscope objective scoring
0	No staining or less than 1 dot in every 10 cells (40X magnification)
1	1-3 dots/cell (visible at 20-40X magnification)
2	4-10 dots/cell. Very few dot clusters (visible at 20-40X magnification)
3	> 10 dots/cell. Less than 10% positive cells have dot clusters (visible at 20X magnification)
4	> 10 dots/cell. More than 10% positive cells have dot clusters (visible at 20X magnification)

Figure S3

ONLINE SUPPLEMENTAL MATERIAL

Index

- Supplemental tables description
- Supplemental Figure Legends
- Materials and Methods
- References to Supplemental Material

Lupo F, *et al. Gut* 2024;0:1–15. doi: 10.1136/gutjnl-2023-329807

SUPPLEMENTAL TABLES DESCRIPTION

Table S1. List of differentially expressed genes upon *Sema3a* overexpression in FC1199 cells.

Table S2. Gene-set enrichment analysis (GSEA) on the list of differentially expressed genes upon Sema3a overexpression in FC1199 cells. Terms highlighted in yellow are reported in the relative figures.

Table S3. List of differentially expressed genes upon *Sema3a* knock-out in FC1199 cells.

Table S4. Gene-set enrichment analysis (GSEA) on the list of differentially expressed genes upon Sema3a knockout in FC1199 cells. Terms highlighted in yellow are reported in the relative figures.

Table S5. List of differentially expressed genes from the comparison between SEMA3A high and low tumors of the ICGC cohort.

Table S6. GSEA analysis on the list of differentially expressed genes from Table S5. Terms highlighted in yellow are reported in the relative figures.

Table S7. List of differentially expressed genes from the comparison between SEMA3A high and low tumors of the PanCuRx cohort.

Table S8. GSEA analysis on the list of differentially expressed genes from Table S7. Terms highlighted in yellow are reported in the relative figures.

Table S9. List of differentially expressed genes from mRNA-seq analysis of tissues from Sema3a proficient and deficient tumors.

Table S10. Gene-set enrichment analysis (GSEA) on the list of differentially expressed genes from Table S9. Terms highlighted in yellow are reported in the relative figures.

Table S11. Custom Macrophages' gene expression signatures.

Lupo F, *et al. Gut* 2024;0:1–15. doi: 10.1136/gutjnl-2023-329807

SUPPLEMENTAL FIGURE LEGENDS

Supplementary Figure 1. Regulation of *Sema3a* and *Sema3c* expression by cell intrinsic and cell extrinsic inputs. A. Boxplot of Semaphorins Z-scores stratified by the Moffitt subtypes [1] in the TCGA [2], the ICGC [3], and the PanCuRx [4] cohorts. *, $p < 0.05$; **, $p < 0.01$; and ***, $p < 0.001$ by Student t test. Only Semaphorins whose expression could be detected in all the transcriptomic datasets are shown; the Semaphorin genes displayed in Figure 1A are in red colored font. **B**. Heatmap showing correlation (Spearman's correlation) between the indicated Semaphorins and basal-like/squamous associated gene programs in the PanCuRx[4] and the TCGA[2] cohorts. All annotated boxes, $p < 0.05$. **C.** Scatterplot showing the correlation between expression level of SEMA3A and samples "basalness" score in PDOs (n=16) (computed as ssgsea_Moffitt_Basal_score-ssgsea_Moffitt_Classical_score). **D**. qPCR analysis of *Sema3a* and *Sema3c* expression in mN (n = 3), mP (n=3), mT (n=6), and mM (n = 3) organoids. Results are shown as mean ± SD. *, $p < 0.05$ as determined by Student's *t*-test. **E.** Immunoblot analysis of SEMA3A in whole cell lysates from mN, mP, mT, and mM organoids. β-actin was used as loading control (left panel). Reported below the immunoblot, the *Kras* and *Trp53* status of the cultures. Middle panel, scatter dot plot showing the quantification of SEMA3A from the immunoblot on the right. *, $p < 0.05$ by Student t test. Right panel, levels of SEMA3A detected in the secretome of mouse organoid cultures using an ELISA assay. **, $p < 0.01$; *, $p < 0.05$; and 0.08 by Student t test. **F.** Snapshot of the gel-like image output of the DNA-chip bioanalyzer run showing the loss of the *Trp53* wild-type allele upon Nutlin-3A treatment (see methods) of mT6. Arrowheads indicate the bands corresponding to either wild-type or mutant Trp53. **G**. qPCR analysis of *Sema3c* in mouse tumor organoids displaying loss-of-heterozygosity of p53 compared to the parental culture. **H.** Left panel, immunoblot analysis of TP53 and SEMA3A in whole cell lysates of cell lines established from KPshP53 mice treated with vehicle or Doxycicline. GAPDH, loading control. Right panel, changes in the expression (qPCR) of *Sema3a* detected in KPshP53 derived cell lines following Doxycicline treatment. **I**. Snapshot of the gel-like image output of the DNA-chip bioanalyzer run showing the lack of the *Trp53* wild-type allele in FC1199, FC1245, and FC1242 cell lines. mT6 organoids were used as control for the presence of both wild-type and mutant allele. **J.** Anti-p63 ChIP-qPCR analysis of 3 different genomic regions of the *Krt5* promoter from mouse PDAC cells (FC1199) transduced with either empty control (NTC) or p63 ORF. On the right, anti-IgG Chip-qPCR of the 7 genomic regions of Figure 1G. **K.** Changes in the expression levels of *Kras, Sema3c, Sema3a, Nqo1,* and *Rpa3* in mouse PDAC cell lines transfected with empty vector or two different siRNAs targeting the mutant Kras allele. Results are shown as mean ± S.D. of 4 independent experiments. **, $p < 0.01$; and *, $p < 0.05$ by Student t test. **L**. Immunoblot analysis of SMAD4 in mouse tumor organoids transduced with empty vector or with shRNAs (#1 and #2) targeting SMAD4. GAPDH was used as loading control. Right panel, ELISA of SEMA3a in mT6 organoids treated as indicated (shown is the average of two independent experiments).

Supplementary Figure 2. Expression of SEMA3A in PDAC tissues. A. Boxplot showing expression of *SEMA3A* in TCGA PDAC tissue versus normal tissue from TCGA and GTEx. * $p < 0.01$. Statistical significance was assessed by Student's t-test. **B.** Stacked

bar plot showing the molecular subtypes distribution according to the *SEMA3A* expression status (see methods) in the PanCuRx [4] cohort. **C.** Stacked bar plots showing the distribution of *KRAS* genetic status according to the expression of *SEMA3A* in the PanCuRx [4] dataset. **D**. UMAP plot showing the integration of individual cells from the 4 distinct PDAC dataset [4, 5, 6, 7] and annotated in 9 different cell clusters. Different cell types are color-coded. **E** Copy-number analysis of the ductal cell cluster. The UMAP plot shows ductal cells colored according to the copy-number profile (red, aneuploid; green, diploid; blue, not determined). **F**. UMAP plot of cells from the stromal clusters. Cells were classified as CAFs based on the expression of known markers. All other cell clusters were excluded from further analysis. **G.** Violin plots of normalized expression of *NRP1* and *PLXNA1* in each annotated cell cluster from 4 different scRNA-seq datasets. **H.** Samples from the harmonized scRNA-seq dataset ranked from left to right based on the proportion of basal-like or classical cells. For the analysis in Figure 2D, we considered the cells from the cases in blue (n = 4) and red (n = 4) which show the highest proportion of basal-like and classical cells, respectively. **I**. On the left, normalized expression of *Sema3a* in epithelial and stromal cell clusters from the scRNA-seq data of Elyada and colleagues [8]. On the right, expression of *Sema3a* in mouse PDAC cells classified as either classical or basal-like. ****, $p < 0.0001$ by Wilcoxon Mann Whitney.

Supplementary Figure 3. Epithelial expression of SEMA3A is enriched in basal-like PDAC.A. Representative immunohistochemical images of heterogeneous PDAC tissue displaying the presence of both classical (GATA6+ S100A2-) and basal-like (GATA6- S100A2+) cells. Scale bars, 100 μm. **B** Representative ISH images showing neoplastic epithelial cells which were scored as either negative (left panels) or positive (right panels) for *SEMA3A*. A magnification for each area is provided. Scale bars, 50 μm. Lower panel, table reporting the criteria for scoring ISH staining based on indication from vendor (see also methods).

Supplementary Figure 4. Modulation of SEMA3A and associated changes in MAPK pathway activation. A. Immunoblot analysis of N-cadherin, Vimentin and ZEB1 in FC1242, FC1245 and FC1199 cells. β-actin was used as loading control. On top, heatmap of the Collison signatures derived ssgsea score [9] for the three KPC derived cell lines. RNA-seq data from [10]. **B.** qPCR analysis of *Sema3a* in parental KPC cell lines and derived subclones. **, $p < 0.01$ by Student t test. **C.** qPCR analysis of *Sema3a* in mT6 after transduction with a vector carrying *Sema3a* ORF (OE, left panel), and in mM3L following stable transduction with two different gRNAs targeting *Sema3a* (KO, right panels). ***, $p < 0.001$; *, $p < 0.05$ by Student t test. **D**. qPCR analysis of *Sema3a* in two different KPC cell lines following transduction with a vector carrying the *Sema3a* ORF. ***, $p < 0.001$; *, $p < 0.05$ by Student t test. **E**. qPCR analysis of *Sema3a* in FC1199A cell line following knockout with two different gRNAs targeting *Sema3a.* **, $p < 0.01$ by Student t test. **F**. Levels of secreted SEMA3A assayed by ELISA in the conditioned media from mT6 (CTR and OE) and mM3L (NTC and KO). **G**. Immunoblot analyses of the indicated proteins in whole cell lysates from mouse organoid cultures (mT6 and mM3L) cultivated in either organoid medium or in minimal medium. GAPDH used as loading control is the same as in Figure 3G. **H**. Bar plots showing the quantification of changes in the phosphorylated levels of p-ERK1 (upper panel) and p-ERK2 (lower panel) as relative

density of the total protein level. Data presented as means ± SD of three biological replicates. *, $p < 0.05$ by Student's *t*-test corrected for multiple comparison using the Holm-Sidak method. **I** Immunoblot analyses of the indicated proteins in whole cell lysates from mouse pancreatic cancer cell lines following either overexpression (OE) or genetic knockdown (KO) of SEMA3A. GAPDH used as loading control is the same displayed in Figure 3I. **J**. Bar plots showing the quantification of changes in the phosphorylated levels of p-ERK1 (upper panel) and p-ERK2 (lower panel) as relative density of the total protein level. Data presented as means ± SD of three biological replicates. **, $p < 0.01$; *, $p < 0.05$ by Student's *t*-test corrected for multiple comparison using the Holm-Sidak method.

Supplementary Figure 5. SEMA3A promotes anoikis resistance A. Immunoblot analysis of Vimentin and E-cadherin in whole cell lysates from organoid cultures (mT6 and mM3L) cultivated in either organoid or minimal medium. GAPDH used as loading control is the same displayed in Figure 3G and Supplementary Figure 4G. **B**. Bar plot showing the quantification of changes in Vimentin (left panel) and E-cadherin (right panel) levels. Data presented as means ± SD of three biological replicates. ***, $p < 0.001$; **, $p < 0.01$; *, $p < 0.05$ by Student's *t*-test corrected for multiple comparison using the Holm-Sidak method. **C**. qPCR analysis of *Sema3a*, *Snai1*, and *Zeb1* expression in mT6 organoid cultures with (OE) and without (CTR) forced expression of Sema3a and treated as indicated for 5 days **D**. qPCR analysis of *Sema3a*, *Snai1*, and *Zeb1* expression in mM3L organoid cultures with (3A3-KO) and without (NTC) deletion of *Sema3a* and treated as indicated for for 5 days. in C and D, ****, $p < 0.0001$; ***, $p < 0.001$; **, $p < 0.01$; and *, $p < 0.05$ by Student t test. **E.** Immunoblot analysis of Vimentin and E-cadherin in whole cell lysates from pancreatic cancer cell lines following overexpression (OE) or knockout (KO) of SEMA3A. GAPDH used as loading control is the same displayed in Figure 3I and Supplementary Figure 4I. **F.** Bar plot showing the quantification of changes in Vimentin (left panel) and E-cadherin (right panel) levels. Data presented as means ± SD of three biological replicates. **G.** Quantification of the anoikis assay (% of cleaved Caspase 3/7 positive cells) for the FC1199 wild type and knockdown for either *Nrp1* or *Plxna1* in the presence or absence of RhoK inhibitor (RKi) and recombinant SEMA3A (S3A-FC). Indicated the fold change (FC)± S.D. between treated/untreated for each genotype. **, $p < 0.01$ by Student t test. **H.** Left panel, immunoblot analysis of NRP1, pFak (Y397), Fak, pAkt, Akt, pErk 1/2 and Erk 1/2 in whole cell lysates from FC1199 *Sema3A* proficient transfected with either non-targeting control (NTC) of siRNA targeting *Nrp1.* GAPDH was used as loading control. Right panel, immunoblot analysis of PLXNA1, pFak (Y397), Fak, pAkt, Akt, pErk 1/2 and Erk 1/2 in whole cell lysates from FC1199 *Sema3A* proficient transfected with either non-targeting control (NTC) of siRNA targeting *Plxna1.* GAPDH was used as loading control. **I.** Quantification of the anoikis assay (% of cleaved Caspase3/7 positive cells) for the mM3L wild-type and knockout for *Sema3a* in the presence or the absence of the FAK inhibitor defactinib. Indicated the fold change (FC)± S.D. between treated/untreated for each genotype. **, $p < 0.01$ by Student t test.

Supplementary Figure 6. *In vivo* effect of SEMA3A perturbation. A. Scatter plot displaying tumor weight (gr) at endpoint in the FC1199A cohort. *, $p < 0.05$ by Student t test. **B.** Scatter dot plot displaying tumor volumes (measured using Vevo 2100 System) in mice transplanted with FC1245 cells (n = 5/group) displaying different levels of

SEMA3A expression. Data are displayed as means ± S.D. **, p < 0.01; *, p < 0.05 by Student t test. Middle panel, H&E of whole pancreata from tumor bearing mice; scale bar, 5 mm. On the right, scatter dot plot displaying (means ± S.D) the weight (gr) of tumor masses from the FC1245 cohort. ***, p<0.001 by Student t test. **C.** Scatter plot displaying tumor weight (gr) at endpoint from mM3L organoids transplanted in the pancreata of immunocompetent mice. Means ± S.D. are shown. ****, p < 0.0001 by Student t test. On the right, H&E of whole pancreata from tumor bearing mice. **D.** Volcano plot of the differences in gene expression between control (NTC, n = 3) and *Sema3a* knockout models (KO, n = 3). Indicated are some of the genes with log2FC expression and adjusted $p < 0.05$. Provided in the box is the number of totals, upregulated (red), and downregulated (blue) genes. See Supplemental Table 9 for the full list of differentially expressed genes. **E.** Representative immunohistochemical staining for CD3, CD8, and F4/80 of pancreatic tissues from mice transplanted with FC1199A stably transduced with either mock (CTR) or a vector carrying *Sema3a* ORF (OE). Scale bars, 50 μm. Quantification is provided on the left as mean ± S.D. (see methods). At least five individual areas per case and a minimum of five mice/arm were evaluated. **F.** FACS analysis of tumor tissues from FC1199 NTC, KO and OE showing: % of $F4/80^+CD206^+$, $Ly6G^+$, and $Ly6C^+$ calculated as the percentage of $CD11b^+$ cells; and % of $CD3^+CD8^+$ and $Foxp3^+CD4^+$ calculated as the percentage of $CD45^+$ cells. ***, $p < 0.001$; **, $p < 0.01$ by Student t test. **G.** Boxplot of tumor associated macrophage signature scores in tumors from the ICGC cohort [3] according to the expression of SEMA3A. p-values, Wilcoxon rank-sum test. ****, p < 0.0001; ***, p < 0.001; and **, p < 0.01. See also Supplementary Table 11.

Supplementary Figure 7. Increased intra-tumoral infiltration of TAMs contribute to the aggressive behavior of SEMA3A high tumors. A. qPCR analysis of M1 (Nos2) and M2 (Arg1, Fizz) markers following polarization of RAW 264.7 cells as described in the method section. **B.** qPCR analysis of *CD80*, *CD86* and *CD206* in bone-marrow derived monocytes treated with vehicle (-) or recombinant SEMA3A (+) (100 ng/mL) for 72 hours. Experiment was performed twice, and data are shown as mean value relative the untreated cells. **C.** qPCR analysis of *Nos2*, *Fizz*, *Arg1* in bone-marrow derived monocytes treated with vehicle (-) or recombinant SEMA3A (+) (100 ng/mL) for 72 hours. Data are shown as mean ± S.D of three independent experiments. Statistical significance by Student t test: *, p < 0.05. **D**. Left panel, representative immunofluorescence staining for the M2-like marker CD206 (red) in tumor tissues from either FC1199A or mM3L depleted for *Sema3a* (KO) along with their control (NTC). Right panel, representative staining for CD206 in tumor tissues from FC1199 overexpressing *Sema3a* (OE) along with their control (CTR). Nuclei were stained with DAPI. Scale bars 100 μm. Quantification is provided on the right of the images as relative fluorescence intensity (mean ± S.D.). At least three individual areas per case and a minimum of five mice/arm were evaluated. ***, p < 0.001; **, p < 0.01; and *, p < 0.05 by unpaired Student t test. **E**. Experimental design for the evaluation of CSF1R monoclonal antibody in a mouse model of PDAC. **F**. The effect of CSF1R inhibition on the depletion of monocytes in the blood circulation. *, p < 0.01 by Student t test. **G**. Experimental design for the survival study of tumor-bearing mice treated with vehicle (IgG), CSF1R monoclonal antibody, Gemcitabine, or combination of CSF1Ri and Gem. **H**. Kaplan-Meier survival analysis of mice transplanted

with SEMA3A low cells and treated with control IgG (Ctrl, n = 10), Gemcitabine (Gem, n = 10), αCSF1R (CSF1Ri, n = 10), or combination of Gemcitabine and α CSF1R (GC, n = 10). Statistical differences identified by log-rank test. **I.** Line graph showing tumor volumes (mm^3) of pancreatic masses detected in mice transplanted with SEMA3A control and overexpressing cells treated with αCD8 (CD8, n = 10), Gemcitabine (Gem, n = 10), αCSF1R (CSF1Ri, n = 10), or combination of Gemcitabine and αCSF1R (GC, n = 10).

MATERIALS AND METHODS

Human Samples

Fresh and formalin-fixed and paraffin-embedded (FFPE) PDAC tissues used in this study were obtained from surgical resection of patients treated at the University and Hospital Trust of Verona (Azienda Ospedaliera Universitaria Integrata, AOUI). All tissue specimens were acquired from treatment-naive patients and written informed consent from the donors for research use of the tissue was obtained prior to acquisition of the specimens. FFPE tissue of 11 individual PDAC cases was retrieved from the ARC-Net Biobank and were collected under the protocol number 1885 approved by the local Ethics Committee (*Comitato Etico Azienda Ospedaliera Universitaria Integrata*) to A.S (Prot. 52070, Prog. 1885 on 17/11/2010). These specimens were used for *in situ* hybridization and immunohistochemical analyses. Fresh tissue from curative resections was used for the generation of organoids and was collected under the protocol number 1911 approved by the local Ethics Committee (Comitato Etico Azienda Ospedaliera Universitaria Integrata) to V.C. (Prot. n 61413, Prog 1911 on 19/09/2018). All experiments were conducted in accordance with relevant guidelines and regulations.

Cell lines, organoids, and culture conditions

A total of 10 human pancreatic cancer cell lines were used in this study. The human PDAC cell lines HPAF-II, PANC1, and AsPC-1 were purchased from ATCC (CRL-1997, CRL-1469, CRL-1682). SUIT-2, Hs766T, L3.6pL, COLO 357, and BxPC3 cell lines were kindly provided by Prof. Aldo Scarpa (University of Verona). MIA PaCa-2 was kindly provided by Prof. Vincenzo Bronte (University of Verona). hF2-2D (monolayer) was kindly provided by Dr. David A. Tuveson (Cold Spring Harbor Laboratory, USA). HPAF-II, SUIT-2, PANC-1, L3.6PL, COLO 357, BxPC3 and MIA PaCa-2 were grown in DMEM (Gibco) supplemented with 10% FBS and 1% Penicillin-Streptomycin (Pen-Strep, Gibco). Hs766T, AsPC-1, and hF2-2D were cultured in RPMI (Gibco) supplemented with 10% FBS and 1% Pen-Strep. The two mouse PDAC cell lines used herein (FC1199 and FC1245) were established from tumor tissues of KPC (*Kras*$^{LSL\text{-}G12D/+}$;*Trp53*$^{LSL\text{-}R172H/+}$;*Pdx-1*-Cre) mice [11] and grown in DMEM supplemented with 10% FBS and 1% Penicillin-Streptomycin (Pen-Strep, Gibco). Human (n = 5) and mouse (n = 12) pancreatic organoids were established as previously described [12, 13]. For certain experiments, organoids were adapted to grow either on plastic or embedded in Rat Tail Collagen I (Corning, 354236) prepared according to the manufacturer' s instruction. Human PDAC organoids were cultivated in growth factor reduced Matrigel$^{(R)}$ and overlaid in human complete medium [12]. Mouse organoids were established from normal pancreata, pancreatic tissues containing preinvasive lesions or full-blown carcinomas, and from metastatic tissues. Culture conditions for mouse pancreatic organoids are described in Hutch et al.[13].

Four of the five organoid models used were acquired as part of the Human Cancer Model Initiative (HCMI) https://ocg.cancer.gov/programs/HCMI and, those models are available for access from ATCC. The corresponding IDs are as follows:

Sample Code	ID
PDA1-O	HCM-CSHL-0080-C25
PDA2-O	HCM-CSHL-0077-C25
PDA9-O	HCM-CSHL-0081-C25
PDA20-O	HCM-CSHL-0092-C25

Both monolayer cell cultures and organoids were routinely tested for the presence of mycoplasma using MycoAlert Detection Kit from Lonza, in accordance with the manufacturer's instructions. The cultures were routinely cultured at 37°C with 5% CO_2. To grow cells in hypoxic conditions (5% or 3% O_2), cells were placed in an incubator that provides nitrogen in addition to CO_2 (Heracell 150i, ThermoFisher Scientific). Early-passage mouse tumor organoids were cultured in complete media supplemented with Nutlin-3a (10μM, Sigma-Aldrich) and propagated for at least 3 passages to generate cultures with bi-allelic alteration of p53 [14]. To induce epithelial-to-mesenchymal transition in organoids cultures, 5 ng/mL of TGF-β1 (Preprotech) was added to the culture media (depleted for A83-01 and mNoggin) for 5 days.

Animal studies

C57BL/6J and *NSG* (NOD.Cg-Prkdc^{scid};Il2rg^{tm1Wjl}) mice were purchased from Charles River Laboratory (Milan). All animal experiments regarding transplanted mice were conducted in accordance with procedures approved by CIRSAL at University of Verona (approved project 655/2017-PR, 260/2023-PR); to minimize potential pain, distress, or suffering of the animals, humane endpoints criteria were applied, as required from CIRSAL at University of Verona. For transplantation experiments, 6- to 8-week syngeneic C57BL/6J or immunodeficient NSG mice were used. For orthotopic transplantation, either cell lines ($1x10^5$ cells) or dissociated organoids ($1x10^6$ cells) were resuspended in 50 μL of a 2:3 dilution of Matrigel$^{(R)}$ (Corning) and cold PBS (Gibco) and injected into the tail region of the pancreas using insulin syringes (BD micro-fine 30 Gauge). The injection was considered successful by the development of bubble without signs of leakage. Monitoring of tumor growth was performed as previously described [15]. Briefly, following weekly manual palpation starting 7 days following transplantation, tumor-bearing mice were subjected to high-contrast ultrasound screening using the Vevo 2100 System with a MS250, 13–24 MHz scanhead (Visual Sonics). Mice were sacrificed at the indicated time points. Pancreas, spleen, lungs, and liver were collected for downstream analysis. For tail vein injection**,** cell lines ($1x10^5$ cells) were resuspended in 100 μL of PBS and injected in the lateral caudal vein using insulin syringes (BD micro-fine 30 Gauge). For intrasplenic injection, $1x10^5$ cells were resuspended in 50 μL of cold PBS and injected into the spleen using insulin syringes with a 27-gauge hypodermic needle; mice were then splenectomized. Mice were sacrificed at the indicated time points.

Lentiviral infection of cell lines and organoids

To knock out *Sema3a* in mouse PDAC organoids and cell lines, we used an inducible Crispr/Cas9 lentiviral system. First, both organoids and cell lines were transduced with an Edit-R Inducible Lentiviral hEF1a-Blast-Cas9 Nuclease Particles (Dharmacon,

FE5VCAS11227) followed by selection with 5 µg/mL of blasticidin (Gibco). Three predesigned single-guide RNA (sgRNA) targeting *Sema3a,* and an individual sgRNA non-targeting control (NTC) were acquired from Dharmacon. For the transduction of monolayer cell cultures, 70-80% confluent cultures were incubated in complete transduction media (DMEM, 10% FBS, 1% P/S), lentiviral particles (MOI 10) and 1X polybrene (Santa Cruz Biotechnology); two days after the infection, 2 µg/mL of puromycin (Gibco) was added for selection. For organoids infection, cells were released from Matrigel® using 2mg/mL Dispase I for 20 minutes at 37°C. To obtain single cells, organoids were then enzymatically digested with TripLE (Gibco) supplemented with 2mg/mL Dispase I and 0.1 mg/mL DNAse I (Sigma-Aldrich) for 20 minutes at 37°C. $1x10^5$ cells were then incubated with transduction media (DMEM, 5% FBS, 1% P/S) supplemented with 1 µg/mL polybrene and lentiviral particles (MOI 10) and spinoculated for 1h at RT; cells were then incubated at 37°C for 16 hours and subsequently collected and embedded in 50 µL of Matrigel®. Two days after infection, cultures were treated with 2 µg/mL puromycin (Gibco) for antibiotic selection. Cas9 expression was induced by treating the cultures with 2.5 ng/mL of doxycycline for 3 days. Induction of Cas9 expression was evaluated by western blot using a mouse monoclonal antibody from Cell Signaling (clone 7A9-3A3, #14697). Successful editing and knock out were evaluated by Surveyor® Mutation Detection Kit (Integrated DNA Technologies) and western blotting, respectively. Given the link between *SEMA3A* expression and the TGF-β pathway, *Sema3a* mutant organoids were selected by withdrawal of TGF-β inhibitors (A83-01 and mNoggin) from the culture medium. To overexpress *Sema3a* in mouse PDAC organoids and cell lines, we used a lentiviral vector carrying an open-reading frame for SEMA3A (tagged with MYC-DKK Origene, MR210565L3). LentiORF control particles of pLenti-C-Myc-DDK-P2A-Puro (Origene, PS100092V) were used as NTC, Lentiviral particles were packed in HEK293T cells transfected with plasmid containing the open-reading frame and the packaging plasmid VSV-G with X-tremeGENE9 (Roche, 063665110101). Lentiviral particles were collected two days after the infection by harvesting the viral surnatant, filtered and centrifuged to remove debris. Lentiviral particles were concentrated using Lenti-X concentrator (TaKaRa Bio) and viral titer was determined using Lenti-X qRT-PCR Titration Kit (TaKaRa Bio). Monolayer cell cultures transduction was performed by adding the viral supernatants supplemented with 1 µg/mL of Polybrene to cells having 50-60% of confluency. Antibiotic selection was started after 48 hours using 2 µg/mL of puromycin. Successful overexpression was assessed by Western blot. To knock down *Smad4* in mouse organoids, two shRNAs targeting *Smad4* were used. The vector TRC2 pLKO.5-puro (Sigma-Aldrich) was used as NTC. Organoids' infection was performed as described; two days after infection, cultures were treated with 2 µg/mL puromycin for antibiotic selection. Successful overexpression was assessed by western blot. To overexpress *Trp63* in mouse cultures, we used a lentiviral vector carrying an ORF for *Trp63* (mGFP-tagged; Origene, MR227530L4). Lentiviral particles production and monolayer cell cultures infection were performed as previously described. Successful overexpression was assessed by western blot.

sgRNA targeting *Sema3a*

sgRNA code	Sequence

3A1	GGAACTGCTGCGGACTTCAT
3A2	GTAAGGCACCCACTGATAGT
3A3	GATCAAGACCGGATATATGT

shRNA targeting *Smad4*

shRNA code	**Sequence**
sh1	TCAGGTAGGAGAGAGACGTTTAA
sh2	GCGATTGTGCATTCTCAGGAT

Histology and Immunohistochemistry

Both mouse and human tissues were fixed in 10% neutral buffered formalin and embedded in paraffin. Sections were subjected to Hematoxylin and Eosin as well as immunohistochemical staining. The following primary antibodies were used for immunohistochemical staining of human tissues: S100A2 [EPR5392] (109494, Abcam), GATA-6 (AF1700, Bio-techne). The following primary antibody were used for immunohistochemical staining of mouse tissues: CD3e (SP7) (MA1-90582, Thermo Fisher), CD8a (4SM15) (14-0808-82, Invitrogen), F4/80 (ab6640, Abcam). Slides were scanned at 40x magnification and digitalized using the Aperio Scan-Scope XT Slide Scanner (Aperio Technologies). Quantification of CD3e, CD8a and F4/80 staining was performed in at least five random nonoverlapping fields of visualization (magnification, 20x) in each sample. To quantify CD3e and CD8a positive T cells, DAB positive cells were counted using the Aperio Image Scope software. To measure the percentage of positive F4/80 cells, captured images were first color deconvoluted and DAB+ particles counted automatically using ImageJ. Immunofluorescent staining of mouse tumor tissue was performed using Anti-mannose receptor antibody (CD206) (ab64693, Abcam). Slides were incubated with specific secondary antibody at a 1:500 dilution: Goat anti-Rabbit IgG Alexa Fluor Plus 555 (A32732, Invitrogen). Slides were then incubated with 0.1% Sudan Black B (Carlo Erba) in 70% ethanol for 20 min to reduce non-specific staining. Nuclei were stained using DAPI (D9542, Sigma-Aldrich). Images were captured with Leica TCS SP5 AOBS confocal system. Quantification was performed with ImageJ by measuring relative fluorescence of $CD206^+$ cells in at least three nonoverlapping fields.

In situ hybridization

The *in-situ* hybridization (ISH) was performed on 4 µm section of human PDAC tissues (n = 11). Briefly, sections were deparaffinized by incubation with xylene for 10 minutes, 100% ethanol for 2 minutes and then let dry for 5 minutes at room temperature. Slides were incubated for 10 minutes with RNAscope® Hydrogen Peroxide (Advanced Cell Diagnostics), washed with distilled water and incubated for 20 minutes at 99°C with RNAscope® 1X Retrieval Reagents (Advanced Cell Diagnostics). Sections were rinsed in distilled water and dehydrated in 100% ethanol for 3 minutes and let dry at room temperature. Then, the slides were incubated at 40°C for 10 minutes with RNAscope® Protease Plus (Advanced Cell Diagnostics), washed with distilled water and incubated with the appropriate probe for 2 hours at 40°C, followed by washes with RNAscope® 1X Wash Buffer (Advanced Cell Diagnostic). The different RNAscope® 2.5 HD AMPs (Hs-

SEMA3A-C1, Hs-PLXNA1-C2 and Hs-KRT18-C2 Advanced Cell Diagnostics) were added to the slides following manufacturer's instructions. Positive control probe Hs-UBC and 2-plex negative control probe (Advanced Cell Diagnostics) were used as positive and negative control, respectively. Then, slides were incubated for 10 minutes at room temperature with either RNAscope® 2.5 HD Detection Reagent- RED or GREEN (Advanced Cell Diagnostic). Slides were stained with hematoxylin, dried at 60°C for 15 minutes and mounted with VectaMount® mounting medium (Vector Laboratories). Slides were scanned at 40x magnification and digitalized using the Aperio Scan-Scope XT Slide Scanner. ISH quantification of SEMA3A positive areas (Classical n=18, Basal like n=11) was performed by manual counting based on indication from vendor: 0: No staining or less than 1 dot in every 10 cells (40X magnification); 1+: 1-3 dots/cell (visible at 20-40X magnification); 2+: 4-10 dots/cell, very few dot clusters (visible at 20-40X magnification); 3+: >10 dots/cell, and less than 10% positive cells have dot clusters (visible at 20X magnification); and 4+: >10 dots/cell, and more than 10% positive cells have dot clusters (visible at 20X magnification).

***In vitro* macrophages generation**

To isolate murine bone-marrow (BM) derived monocytes, we collected tibiae and femurs from 6 to 8-weeks old C57BL/6 mice and flushed BM cells. Red blood cells were lysed using a hypotonic solution (8.3% NH4Cl, 1% KHCO3 and 0.5M EDTA) [16]. $1,5*10^6$ BM derived cells were grown in RPMI 1640 (Euroclone) supplemented with 40 ng/mL IL-6 (Miltenyi Biotec, 130-096-686), 40 ng/mL GM-CSF (Miltenyi Biotec, 130-095-735), 10% FBS (Gibco), 2mM L-glutamine (Euroclone), 10mM HEPES (Euroclone), 1mM sodium pyruvate (Euroclone), 150U/mL streptomycin, 200U/mL penicillin/streptomycin. Cultures were maintained at 37°C in 5% CO_2-humidified atmosphere for 4 days. Macrophage's differentiation was promoted by growing BM derived cells in RPMI 1640 supplemented with 100ng/mL CSF-1 (Miltenyi Biotec, 130-101-706), 10% FBS, 2mM L-glutamine, 10mM HEPES, 1mM sodium pyruvate, 1% Pen/Strep [17]. Cells were grown for 7 days at 37°C in 5% CO_2-humidified atmosphere. On day 4 of the culture, fresh cytokine-supplemented complete medium was added. To obtain M1-MΨ or M2-MΨ, macrophages were cultured in presence of IFN-γ (10 U/mL; Miltenyi Biotec, 130-105-773) and LPS (1µg/mL; L8274; Sigma-Aldrich) or IL-4 (10 ng/mL; Miltenyi Biotec, 130-097-758) and IL-13 (10 ng/mL; Miltenyi Biotec, 130-096-688) cytokines-cocktail, respectively. Cells were either left untreated or treated with Recombinant Mouse Semaphorin 3A Fc (5926-S3-025/CF, Biotechne, 100 ng/mL). To analyze macrophages polarization by flow cytometry, the following antibodies were used: anti-F4/80 FITC (Miltenyi Biotec, 130-117-509), anti-CD86 PE (Biolegend, 10-5106), anti-CD206 PerCP Cy5 (Biolegend, 141716), anti-CD80 APC (Biolegend, 104714). Cell viability was assessed using the LIVE/DEADFixable Aqua Dead Cell Stain Kit (Invitrogen, L34966).

***In vitro* macrophages polarization**

Raw 264.7 cells were grown in DMEM supplemented with 10% FBS, 1% pen/strep, 2 mmol/L l-glutamine, 10 mmol/L HEPES. To induce *in vitro* differentiation, cells were stimulated with M-CSF (25 ng/ml) for 48hs, followed by a 72h incubation with IL4 (40 ng/ml) and IL13 (40 ng/ml) to promote M2 polarization or conditioned medium collected

from FC1199 CTR or FC1199 3A-OE cell lines. Unstimulated RAW 264.7 (M0) were used as control.

Transwell migration assay

To assess the chemo-attractant capability of SEMA3A towards macrophages, we performed a transwell migration assay using the cell line RAW264.7 (kindly provided by Prof. Vincenzo Bronte, University of Verona) transiently downregulated for either *Nrp1* or *Plxna1* and NTC. Cells were grown in DMEM supplemented with 10% FBS, 1% pen/strep, 2 mmol/L l-glutamine, 10 mmol/L HEPES and differentiated into M1 or M2 macrophages. To obtain M1 macrophages, cells were stimulated with M-CSF (25 ng/ml) for 48 h, followed by a 72-hour stimulation with IFN γ (0.3 µg/ml) and LPS (1µg/ml). For M2 macrophages polarization, M-CSF stimulation was followed by a 72 h IL4 (40 ng/ml) and IL13 (40 ng/ml) stimulation. Non-stimulated (M0) cells were used as control. To perform the *in vitro* migration assay, we used 8 µm pore transwell (Corning, 353097) coated with 10% Matrigel. Both M1 and M2 polarized RAW264.7, and unstimulated cells, were collected and resuspended in 2% FBS growth medium and seeded on top of the coated transwell [18]. In parallel, the same cells were used to assess macrophages polarization. Growth medium with or without 100 ng/ml SEMA3A-Fc was added on the bottom of the well. Growth medium supplemented with 20% FBS was used as positive control. After 24 h, non-migrated cells were removed from the upper side of the transwell with a cotton swab whereas transwells' membranes were fixed with 3.7% Paraformaldehyde (Sigma Aldrich, 8187081000), stained with crystal violet, and eluted with a solution containing 50% ethanol and 0.1% acetic acid. Absorbance was measured at 595 nm using a microplate reader (BioTek, Synergy 2 Multi-mode Microplate Reader).

***In vivo* treatment experiment**

For *in vivo* treatment with anti-CSF1R, 7-8 weeks old C57BL6/J mice of both sexes were randomized into four groups and treated for 3 days with 300 µg of anti-mouse CSF1R (CD115) [AFS98] (BioXCell, BE0213) or rat IgG2a [2A3] (BioXCell, BE0089) as isotypic control. On day four, mice were orthotopically transplanted with $1*10^5$ FC1199 NTC or FC1199 3A-OE cells. Animals were treated every 2 days and tumor growth was monitored by abdominal palpation and high-contrast ultrasound (Vevo 2100 System). Mice were sacrificed when tumors reached an average volume of approximately 100 mm^3 or at human endpoint, when signs of discomfort were evident. To evaluate the effect of anti-CSF1R treatment on immune cell populations, the peripheral blood from untreated and treated mice was subjected to cytofluorimetric analysis with the following antibodies: anti-CD45.2 APC (Invitrogen, 14-0454-82), anti-CD11b FITC (M1/70) (eBioscience, 11-0112-85), anti-F4/80 PECy7 (BM8) (eBioscience, 25-4801-82), anti-Ly6C V450 (Invitrogen, 48-5932-82), anti-Ly6G APC-H7 (Biolegend, 127624), anti-CD16/32 (Sony,1106510). Cell viability was assessed using the LIVE/DEADFixable Aqua Dead Cell Stain Kit. Samples were acquired with FACS-Canto II (BD). Data were analyzed by FlowJo software (Tree Star, Inc). Survival study was performed using 7-8 weeks old female C57BL6/J mice orthotopically transplanted with $1*10^5$ FC1199 NTC or FC1199 3A-OE cells. On day 10, tumor growth was assessed by abdominal palpation and mice were randomized into 8 groups. Mice were treated 3 times/week with 300 µg of anti-mouse CSF1R (CD115) [AFS98], rat IgG2a [2A3] as isotypic control or 120 mg/kg Gemcitabine once a week. To

evaluate the effect of *in vivo* CD8 + T cells depletion, 7-8 weeks old female C57BL6/J mice were orthotopically transplanted with $1*10^5$ FC1199 NTC, FC1199 3A-OE or FC1199 3A3-KO cells. On day 10, tumor growth was assessed by abdominal palpation and mice were randomized into 6 groups. Mice were treated once every three weeks with 200 µg of monoclonal anti-mouse CD8 (YTS 169.4, BioXCell), 3 times/week with 300 µg of anti-mouse CSF1R (CD115) [AFS98] or 120 mg/kg Gemcitabine once a week. Tumor growth was monitored by abdominal palpation and high-contrast ultrasound (Vevo 2100 System). Mice were sacrificed when tumors reached an average volume of approximately 300 mm^3.

Transient Knockdown in Cell lines

To transiently downregulate the expression of specific genes, cells were transfected with siRNA for *Kras*, *TP63*, *Nrp1, Plxna1* or with scramble control siRNA, and harvested 48 hours later. Mouse cell lines were transfected with 5 nM of ON-TARGET Plus mouse Kras siRNA, SMART pool (horizon, L-043846-01-0005), 25 pmol of siRNA targeting NRP1 (Thermofisher Scientific, 16704, Assay ID: 155679) or Plxna1 (Thermofisher Scientific, 16704, Assay ID:150201). Human cell lines were transfected with 25 pmol of siRNA targeting *TP63* (Thermofisher Scientific, 4392420, Assay ID: s531582) Lipofectamine™ 2000 (Thermofisher Scientific, #11668027) was used for siRNA transfection according to manufacturer's instruction for 6-well plates format.

Cell viability assay

The proliferation of mouse cells following genetic perturbation of *Sema3a* was measured using the CellTiter-Glo assay (Promega, G9683). $1*10^3$ cells were plated on white 96-well plate (Thermofisher Scientific), cultured in 100 µL of culture medium, and viability was measured at endpoint (72 hours) using a microplate reader (BioTek, Synergy 2 Multi-mode Microplate Reader).

Immunoblotting

Whole cell lysates were prepared using Cell Signaling Lysis Buffer (Cell Signaling) and separated on 4-12% Bis-Tris NuPAGE gels (Life Technologies), transferred onto a PVDF membrane (Thermo Scientific) and incubated with the following antibodies: p63 (D9L7L) (39692, Cell Signalling), Sema3a (ab23393, Abcam), Sema3c (MAB1728, bio-techne) Smad4 (B-8/sc-7966, Santa Cruz Biotechnology), phospho-FAK (Tyr-397) (31H5L17/700255, Invitrogen), FAK (3285, Cell Signalling), phospho-Akt (4060, Cell Signalling), Akt (9272, Cell Signalling), ERK1/2 (9102, Cell Signalling), phospho-ERK1/2 (4376, Cell Signalling), E-Cadherin (M3612, Dako), Vimentin (NCL-L-VIM-V9, Leica Biosystems), Nrp1 (ab81321, Abcam), Plxna1 (ab23391, Abcam), p53 (1C12) (2554, Cell Signalling), N-Cadherin (D4R1H) (13116, Cell signaling). GADPH (5174, Cell Signalling) (sc-166545, Santa Cruz Biotechnology) and β-Actin (4967, Cell Signalling) were used as loading control. The immunoblots were visualized with ECL plus (Amersham/GE Healthcare Europe GmgH).

Anoikis and Scratch assays

The anoikis assay was performed on both single cells dissociated from mouse metastatic organoids deficient for *Sema3a,* mouse monolayer cell cultures (FC1199) overexpressing

Sema3a or knocked down for *Nrp1* and *Plxna1.* Cells were plated in Poly(2-hydroxyethyl methacrylate) (sc-253284) coated 96-well plates black/clear flat tc (Corning) ($5*0^3$ cells/well for mouse organoids; $1*10^3$ cells/well for FC1199). Cells were either left untreated or treated with Y-27632 dihydrochloride (Y0503, Sigma-Aldrich, 10,5 µM), Recombinant Mouse Semaphorin 3A Fc (100 ng/mL), or the selective FAK inhibitor Defactinib (Selleckem, 1µM). CellEvent™ Caspase-3/7 Green Detection Reagent (Invitrogen) was added to the cultures at a concentration of 4 µM. After 4 days, Hoechst (1µg/ml, Thermo Fisher) was added to the cultures and incubated for 30 minutes. Images were acquired using the EVOS Cell Imaging System (Thermo Fisher Scientific) and green signal quantification was performed in at least five random nonoverlapping fields using ImageJ. For the scratch assay, FC1199 3A3-KO, FC1199 3A-OE and FC1245 3A-OE monolayer cell cultures were initially plated in DMEM, 10% FBS, 1% P/S in 6-well plates. Once cells reached 80% confluency, the culture medium was replaced with a low-serum medium (2% FBS) and cells cultivated in this condition for additional 24 hours. A 200 µl pipette tip was then used to scrape the cells followed by two consecutive washes with PBS to remove cell debris. Finally, fresh low-serum culture medium was added to the cultures. Recombinant Mouse Semaphorin 3A Fc was used at a final concentration of 100 ng/mL. Brightfield images were taken at 0h, 8h and 24h at a 2.5X magnification.

qRT-PCR analysis

RNA was extracted from cell lines and organoids using the Trizol® Reagent (Life Technologies) method. 1 µg of DNase-treated RNA was reverse transcribed using TaqMan® Reverse Transcription reagents (Applied Biosystems) in a volume of 20 µL according to the manufacturer's instructions. Samples were diluted to a final concentration of 10 ng/µL. For TaqMan-based qRT-PCR. the following probes were used (TaqMan® Gene Expression Assay): *Sema3a* (Mm00436469_m1), *Ctgf* (Mm01192933_g1 *), Zeb1* (Mm00495564_m1), *Snai* (Mm00441533_g1), *Trp63* (Mm00495793_m1), *Smad4* (Mm03023996_m1), *Vegf (*Mm01281449_m1), *Kras* (Mm00517492_m1), *Sema3c* (Mm00443121_m1), *Nqo1* (Mm01253561_m1), *Rpa3* (Mm01165241_g1), *Nrp1* (Mm00435379_m1), *Plxna1* (Mm00501110_m1),TP63 (Hs00978340_m1), SEMA3A (Hs00173810_m1), Hprt1/HPRT1 (Mm03024075_m1, Hs02800695_m1) was used as reference gene was used as reference gene. For SYBR green-based qRT-PCR the following primers were used: *Nos2* (F: GTTCTCAGCCCAACAATACAAGA, R: GTGGACGGGTCGATGTCAC), *Arg1* (F: CTCCAAGCCAAAGTCCTTAGAG, R: AGGAGCTGTCATTAGGGACATC), *Fizz1* (F: TCCCAGTGAATACTGATGAGA, R: CCACTCTGGATCTCCCAAGA), *Hprt1* (F: CTGGTGAAAAGGACCTCTCGAAG, R: CCAGTTTCACTAATGACACAAACG). Relative gene expression quantification was performed using the ΔΔCt method with the Sequence Detection Systems Software, Version 1.9.1 (Applied Biosystems).

Chip qPCR

Mouse cell lines overexpressing *Trp63* ($1X10^7$ cells) were fixed for 10 minutes with 37% formaldehyde, while slowly shaking. Formaldehyde was quenched with 125 mM glycine; medium was removed, and cells were washed with cold PBS. Cells were collected and centrifuged at 1500 rpm for 10 minutes at 4°C. Cell pellet was resuspended in cell lysis buffer (50 mM Tris, pH 8.0, 140 mM NaCl, 1mM EDTA, 10% glycerol, 0,5% NP40, 0,25%

Triton X-100) and incubated for 10 minutes on ice. Cell nuclei were pelleted at 1000 rpm (10 minutes, 4°C) and then resuspended in Nuclei lysis buffer (10 mM Tris pH 8.0, 1mM EDTA, 0,5 mM EGTA, 0,2% SDS), supplemented with protease inhibitors (cOmplete(TM), Mini Protease Inhibitor, Sigma-Aldrich), and incubated for 10 minutes on ice before proceeding to sonication. Nuclei were sonicated by six 15-seconds pulses followed by 45-seconds rest periods (50% maximum potency). Chromatin was then transferred to a 1,5 mL microcentrifuge tube and centrifuged at 8000 rpm for 15 minutes at 4°C. Supernatant was collected for chromatin immunoprecipitation and DNA fragment size evaluation. DNA was extracted using DNeasy Blood & Tissue Kit (Qiagen) and DNA concentration evaluated with Nanodrop 2000 (Life Technologies) and 100 mg of chromatin was used for each reaction. To perform chromatin immunoprecipitation ChIP grade protein A/G plus agarose (50% slurry) was used (Life technologies); chromatin was diluted to a final volume of 300 mL in dilution buffer (10 mM Tris pH 8.0, 0,5 mM EGTA, 1% Triton X-100, 140 mM NaCl) supplemented with protease inhibitors. To preclear chromatin, samples were incubated with 10 mL of protein A/G for 1h at 4°C; samples were then centrifuged at 3000 rpm for 5 minutes at 4°C and the surnatant transferred to a fresh microcentrifuge tube, incubated for 1h at 4°C with p63 (D9L7L) antibody (Cell Signaling Technologies) or normal rabbit IgG (2729S, Cell Signaling Technologies) and then incubated over night at 4°C with 50 mL of protein A/G. To elute immunoprecipitated chromatin, samples were centrifuged for 1 min at 3000 rpm, surnatant was removed and samples were subjected to 4 10 minutes incubation with 1 mL of high-salt wash buffer (2mM EDTA, 20 mM HEPES pH 8.0, 500 mM NaCl, 0,1% SDS, 1% Triton X-100) was added to each sample; beads were then incubated with 300 mL of elution buffer (50 mM Tris pH 8.0, 10 mM EDTA, 1% SDS) supplemented with Proteinase K (20 µg/µL), incubated for 2h at 55°C and then overnight at 65°C to reverse crosslink. Immunoprecipitated chromatin was centrifuged for 5 minutes at room temperature, subjected to purification, and resuspended in Nuclease-free Water (Invitrogen) for qPCR analysis. For qPCR analysis, 7 different loci of the *Sema3a* promoter were targeted (see table below); *Krt5* was used as a positive control for the immunoprecipitation whereas normal rabbit IgG were used as negative control; *Hprt1* was used as housekeeping gene.

Locus name	**Primers sequence**
Sema3a 1	F: ACAAGCCAACTGTGAGAACA R: GATATGCAATGGTGAGGTGGG
Sema3a 2	F: TGTCCAATCACAGATCCCCT R: ACCAACCACACTACCAGCAT
Sema3a 3	F: TCTTGAGGACAGACTGAACCC R: TCATCTCTGTTGTGTCCTGCT
Sema3a 4	F: AGCTCTCTTCGACATAAGGCA R: TGCTCCTCATTATACGGGGT
Sema3a 5	F: AGCTCTCTTCGACATAAGGCA R: CTGACACTCTGCAATTGGGC
Sema3a 6	F: TTAACGCTACCCCACTTCCA R: TGCCGTTGTCACACTTGTTT
Sema3a 7	F: CGTTTGTGCCTAACCCAGAG R: CACAGGCTTCTTTTGCTGGT
Krt5 1	F: TACCCAAGAAAAGAGGCCGT R: CAGCTTTGGGGTTTCTGTCC

Krt5 2	F: CCAGGACACCAGCTCTGTAA R: TAGAAGTGGGTTGGGCAGAG
Krt5 3	F: ATCCTACAGTTCTGGCGGAG R: CGATTTGCAGGTTCAGAGGG
Hprt1	F: CTGGTGAAAAGGACCTCTCGAAG R: CCAGTTTCACTAATGACACAAACG

ELISA

Cell culture supernatants were collected after 3 days of conditioning; particulates were removed by centrifuging samples for 15 minutes at 1000g, 4°C. Plasma from orthotopic mouse models was collected using EDTA 0,5 M as an anticoagulant and centrifuged for 15 minutes at 1000g, 4°C within 30 minutes of collection. ELISA assay was performed using Mouse Semaphorin-3A(SEMA3A) ELISA kit (CUSABIO, CSB-EL020980MO-96) following manufacturer's instructions. Results were calculated using the Curve Expert 1.4 software.

Flow cytometry

Tumor flow cytometry immunophenotyping was performed according already published protocols. Briefly, tumors were minced and digested for 30 minutes at 37°C with a digestive mix containing 1 mg/mL Collagenase IV (17104019, Gibco) , 0.1 mg/mL Hyaluronidase (HX0514, Calbiochem), and 30 U/mL DNAse (D5025-150KU, Sigma aldirch) in RPMI 1640; the cell suspension was separated from the undigested material using a 70-µm cell strainer (431751, Corning). Cells ($1X10^6$) were incubated with the following antibodies according to manufacturer's' instruction: anti-CD45 PE/Cy7 (30-F11) (Biolegend, 103114), anti-Cd11b V500 (BD Biosciences, 562127), anti Ly6c APC-H7 (BD Biosciences, 560596), anti Ly6G PE (BD Biosciences, 551461), anti-CD3 FITC (17A2) (Biolegend, 100204), anti-CD8a PerCP/Cy5.5 (53-6.7) (Biolegend, 100734), anti-F4/80 FITC (REA126) (Miltenyi Biotec, 130-117-509), anti-CD206 PerCP Cy5 (C068C2) (Biolegend, 141716). Cell viability was assessed using the LIVE/DEADFixable Aqua Dead Cell Stain Kit (Invitrogen, L34966).

For Tregs staining, $1X10^6$ cells were incubated with the following antibodies according to manufacturer's' instruction: anti-CD45 PE/Cy7 (30-F11) (Biolegend, 103114), anti-CD3 APC (17A2) (Sony, 1101180), anti-CD8a FITC (53-6.7) (eBioscience, 11-0081-82), anti-CD4 PerCP/Cy5.5 (RM4-5), (eBioscience, 45-0042-82), anti-Foxp3 PE (NRRF-30) (eBioscience, 12-4771-82). Cell viability was assessed using the LIVE/DEADFixable Aqua Dead Cell Stain Kit (Invitrogen, L34966). Cell permeabilization was performed using the Foxp3/Transcription Factor Staining Buffer Set (eBioscience, 00-5523-00).

RNA sequencing

RNA was harvested from monolayer cell cultures using TRIzol (LifeTechnologies), followed by column-based purification with the PureLink RNA Mini Kit (Ambion). To collect RNA from flash-frozen tumor tissues, at least 30 consecutive cryosections (16 µm) for each sample were cut and collected in TRIzol. RNA isolation was performed using the PureLink RNA Mini Kit. The quality of purified RNA was evaluated using a Bioanalyzer 2100 (Agilent) with an RNA 6000 Nano Kit. RNAs with RNA Integrity Number (RIN) values greater than 8 were used for the generation of sequencing libraries using the TruSeq sample Prep Kit V2 (Illumina) according to the manufacturer's instructions. RNA-Seq

libraries prepared from in vitro cultures (n = 12) and from in mouse PDAC tissues (n = 5) were multiplexed and sequenced using a NextSeq 500 platform with single-end reads of 75 bases and a final coverage of 3 million reads per sample. First, we performed quality control and trimming steps, then we aligned reads to the mm10 genome build using Salmon v1.4.0 [19]. Then, we quantified transcripts using the R package tximport v4.0 [20]. Finally, we normalized count data with the R/Biocondutor package DESeq2 v1.30.0 [21], which was also used to identify differentially expressed genes. For gene set enrichment analysis (GSEA), we used the fgsea R package v1.16.0 [22] based on the list of differentially expressed genes sorted by log2 of fold change. We retrieved pathways from MSigDB database and in particular Gene Ontology, KEGG, Biocarta, Reactome and Hallmark gene sets. fgsea function was used with default parameters. Results were considered significant for FDR < 0.05. To classify PDAC cultures and tissues according to the main transcriptomic subtypes [1, 3], we calculated the score for each of the gene sets (i.e., basal-like, classical, pancreatic progenitor, squamous, gene program 2 and gene program 3) using the GSVA R package v1.38.2 [23]. The same package was used to evaluate the enrichment of custom defined immune cell signatures. In both cases, Gsva function was used with ssgsea and gene set scores were compared among different experimental conditions with Wilcoxon rank-sum test.

Analysis of Single-cell RNA-Sequencing data

scRNA-Seq data from normal pancreatic tissues were downloaded from the Seurat V3 repository together with their annotation metadata. The four datasets Muraro et al. [24] (ncells=2285), Segerstolpe et al.[25] (cells = 2394), Grün et al.[26] (ncells = 1004) and Lawlor et al. [27] (ncells = 638) were integrated and queried with the *R* package Seurat V4.0.1 [28]. ScRNA-Seq from human PDAC tissues PDAC tissues were downloaded from NGDC (GSA: CRA001160), GEO (Accession #GSE154778 and #GSE155698) and EGA (accession EGAS00001002543) together with annotation metadata, when provided. The dataset Peng et al.[6] (primary PDAC = 24, ncells = 41964), Lin et al.[5] (primary PDAC = 10, ncells = 7752), Chan-Seng-Yue et al.[4] (primary PDAC = 13, ncells = 33970) and Steele et al.[7] (primary PDAC = 16, ncells = 42844) were first preprocessed individually using Seurat V4.0.1[28] for quality control and filtering (percent_mt_max = 20, nFeature_min = 500, nCount_min = 500, nCount_max = 50000), then integration was performed through *harmony* [29] using default parameters and dataset metadata as grouping variable. The integrated dataset was annotated through *singleR* package using as reference the preloaded dataset *HPCA* from the *celldex* package [30]. Epithelial cells were re-classified as ductal, acinar, or endocrine using known gene signatures [31]. Identification of tumor cells in the ductal cluster, was performed with copycat CNV analysis at sample level, using as normal reference non epithelial cells. Fibroblasts were re-classified using known gene signatures[31]. Single cell RNA-seq normalized counts of fibroblasts enriched dataset from Elyada et al.[8] were downloaded from GEO (GSE129455). The data were imported and managed with Seurat.

Statistical Analysis and data mining

We analyzed three available transcriptomic datasets to explore the correlation between SEMA3A expression and PDAC molecular subtypes. Those cohorts are: the PACA-AU cohort [3] of the ICGC consortium; the TCGA-PAAD cohort [2] of the TCGA consortium

and the PanCuRx cohort [4] (EGA archive accession EGAS00001002543). The ICGC dataset contains normalized expression values (TMM normalized using edgeR Bioconductor package, converted to CPM and log2 transformed) of 96 pancreatic cancer patients. We downloaded associated clinical data from https://dcc.icgc.org/releases/current/Projects/PACA-AU. The TCGA dataset was downloaded from http://firebrowse.org/?cohort=PAAD, and the sample number filtered down to 148, according to a more precise histological revision of included specimens. The PanCuRx dataset was preprocessed with STAR v2.7.6a [32] and RSEM v1.3.1 [33], and eventually a vst expression matrix was produced. Within each cohort, Z-scores standardization of the expression data was performed before subsequent analysis. Expression of SEMA3A was stratified according to tumor stage, subtype classification, and (when available) survival status. The correlation of SEMA3A expression with other genes was evaluated using Spearman's correlation test (significant p-value < 0.001). To classify tumors from the PanCuRx and the ICGC datasets according to the expression of SEMA3A, the distribution of their transcripts levels in the respective cohorts was assessed. We observed a normal distribution for ICGC and TCGA, whereas PanCuRx was bimodal. Thus, we stratified the first two cohorts according to median value of SEMA3A expression. In the PanCuRx dataset instead, we set a threshold at the 3rd quartile which corresponded to 5 (vst).

REFERENCES TO SUPPLEMENTAL MATERIAL

1 Moffitt RA, Marayati R, Flate EL, Volmar KE, Loeza SG, Hoadley KA*, et al.* Virtual microdissection identifies distinct tumor- and stroma-specific subtypes of pancreatic ductal adenocarcinoma. Nat Genet 2015;**47**:1168-78.
2 Cancer Genome Atlas Research Network. Electronic address aadhe, Cancer Genome Atlas Research N. Integrated Genomic Characterization of Pancreatic Ductal Adenocarcinoma. Cancer Cell 2017;**32**:185-203 e13.
3 Bailey P, Chang DK, Nones K, Johns AL, Patch AM, Gingras MC*, et al.* Genomic analyses identify molecular subtypes of pancreatic cancer. Nature 2016;**531**:47-52.
4 Chan-Seng-Yue M, Kim JC, Wilson GW, Ng K, Figueroa EF, O'Kane GM*, et al.* Transcription phenotypes of pancreatic cancer are driven by genomic events during tumor evolution. Nat Genet 2020;**52**:231-40.
5 Lin W, Noel P, Borazanci EH, Lee J, Amini A, Han IW*, et al.* Single-cell transcriptome analysis of tumor and stromal compartments of pancreatic ductal adenocarcinoma primary tumors and metastatic lesions. Genome Med 2020;**12**:80.
6 Peng J, Sun BF, Chen CY, Zhou JY, Chen YS, Chen H*, et al.* Single-cell RNA-seq highlights intra-tumoral heterogeneity and malignant progression in pancreatic ductal adenocarcinoma. Cell Res 2019;**29**:725-38.
7 Steele NG, Carpenter ES, Kemp SB, Sirihorachai V, The S, Delrosario L*, et al.* Multimodal Mapping of the Tumor and Peripheral Blood Immune Landscape in Human Pancreatic Cancer. Nat Cancer 2020;**1**:1097-112.
8 Elyada E, Bolisetty M, Laise P, Flynn WF, Courtois ET, Burkhart RA*, et al.* Cross-Species Single-Cell Analysis of Pancreatic Ductal Adenocarcinoma Reveals Antigen-Presenting Cancer-Associated Fibroblasts. Cancer Discov 2019;**9**:1102-23.
9 Collisson EA, Sadanandam A, Olson P, Gibb WJ, Truitt M, Gu S*, et al.* Subtypes of pancreatic ductal adenocarcinoma and their differing responses to therapy. Nat Med 2011;**17**:500-3.
10 Carbone C, Piro G, Agostini A, Delfino P, De Sanctis F, Nasca V*, et al.* Intratumoral injection of TLR9 agonist promotes an immunopermissive microenvironment transition and causes cooperative antitumor activity in combination with anti-PD1 in pancreatic cancer. J Immunother Cancer 2021;**9**.
11 Hingorani SR, Wang L, Multani AS, Combs C, Deramaudt TB, Hruban RH*, et al.* Trp53R172H and KrasG12D cooperate to promote chromosomal instability and widely metastatic pancreatic ductal adenocarcinoma in mice. Cancer Cell 2005;**7**:469-83.
12 Boj SF, Hwang CI, Baker LA, Chio, II, Engle DD, Corbo V*, et al.* Organoid models of human and mouse ductal pancreatic cancer. Cell 2015;**160**:324-38.
13 Huch M, Bonfanti P, Boj SF, Sato T, Loomans CJ, van de Wetering M*, et al.* Unlimited in vitro expansion of adult bi-potent pancreas progenitors through the Lgr5/R-spondin axis. EMBO J 2013;**32**:2708-21.
14 Oni TE, Biffi G, Baker LA, Hao Y, Tonelli C, Somerville TDD*, et al.* SOAT1 promotes mevalonate pathway dependency in pancreatic cancer. J Exp Med 2020;**217**.
15 Filippini D, Agosto S, Delfino P, Simbolo M, Piro G, Rusev B*, et al.* Immunoevolution of mouse pancreatic organoid isografts from preinvasive to metastatic disease. Sci Rep 2019;**9**:12286.
16 Facciabene A, De Sanctis F, Pierini S, Reis ES, Balint K, Facciponte J*, et al.* Local endothelial complement activation reverses endothelial quiescence, enabling t-cell

homing, and tumor control during t-cell immunotherapy. Oncoimmunology 2017;**6**:e1326442.
17 Solito S, Pinton L, De Sanctis F, Ugel S, Bronte V, Mandruzzato S*, et al.* Methods to Measure MDSC Immune Suppressive Activity In Vitro and In Vivo. Curr Protoc Immunol 2019;**124**:e61.
18 Marigo I, Trovato R, Hofer F, Ingangi V, Desantis G, Leone K*, et al.* Disabled Homolog 2 Controls Prometastatic Activity of Tumor-Associated Macrophages. Cancer Discov 2020;**10**:1758-73.
19 Patro R, Duggal G, Love MI, Irizarry RA, Kingsford C. Salmon provides fast and bias-aware quantification of transcript expression. Nat Methods 2017;**14**:417-9.
20 Soneson C, Love MI, Robinson MD. Differential analyses for RNA-seq: transcript-level estimates improve gene-level inferences. F1000Res 2015;**4**:1521.
21 Love MI, Huber W, Anders S. Moderated estimation of fold change and dispersion for RNA-seq data with DESeq2. Genome Biol 2014;**15**:550.
22 Subramanian A, Tamayo P, Mootha VK, Mukherjee S, Ebert BL, Gillette MA*, et al.* Gene set enrichment analysis: a knowledge-based approach for interpreting genome-wide expression profiles. Proc Natl Acad Sci U S A 2005;**102**:15545-50.
23 Hanzelmann S, Castelo R, Guinney J. GSVA: gene set variation analysis for microarray and RNA-seq data. BMC Bioinformatics 2013;**14**:7.
24 Muraro MJ, Dharmadhikari G, Grun D, Groen N, Dielen T, Jansen E*, et al.* A Single-Cell Transcriptome Atlas of the Human Pancreas. Cell Syst 2016;**3**:385-94 e3.
25 Segerstolpe A, Palasantza A, Eliasson P, Andersson EM, Andreasson AC, Sun X*, et al.* Single-Cell Transcriptome Profiling of Human Pancreatic Islets in Health and Type 2 Diabetes. Cell Metab 2016;**24**:593-607.
26 Grun D, Muraro MJ, Boisset JC, Wiebrands K, Lyubimova A, Dharmadhikari G*, et al.* De Novo Prediction of Stem Cell Identity using Single-Cell Transcriptome Data. Cell Stem Cell 2016;**19**:266-77.
27 Lawlor N, George J, Bolisetty M, Kursawe R, Sun L, Sivakamasundari V*, et al.* Single-cell transcriptomes identify human islet cell signatures and reveal cell-type-specific expression changes in type 2 diabetes. Genome Res 2017;**27**:208-22.
28 Hao Y, Hao S, Andersen-Nissen E, Mauck WM, 3rd, Zheng S, Butler A*, et al.* Integrated analysis of multimodal single-cell data. Cell 2021;**184**:3573-87 e29.
29 Korsunsky I, Millard N, Fan J, Slowikowski K, Zhang F, Wei K*, et al.* Fast, sensitive and accurate integration of single-cell data with Harmony. Nat Methods 2019;**16**:1289-96.
30 Aran D, Looney AP, Liu L, Wu E, Fong V, Hsu A*, et al.* Reference-based analysis of lung single-cell sequencing reveals a transitional profibrotic macrophage. Nat Immunol 2019;**20**:163-72.
31 Franzen O, Gan LM, Bjorkegren JLM. PanglaoDB: a web server for exploration of mouse and human single-cell RNA sequencing data. Database (Oxford) 2019;**2019**.
32 Dobin A, Davis CA, Schlesinger F, Drenkow J, Zaleski C, Jha S*, et al.* STAR: ultrafast universal RNA-seq aligner. Bioinformatics 2013;**29**:15-21.
33 Li B, Dewey CN. RSEM: accurate transcript quantification from RNA-Seq data with or without a reference genome. BMC Bioinformatics 2011;**12**:323.

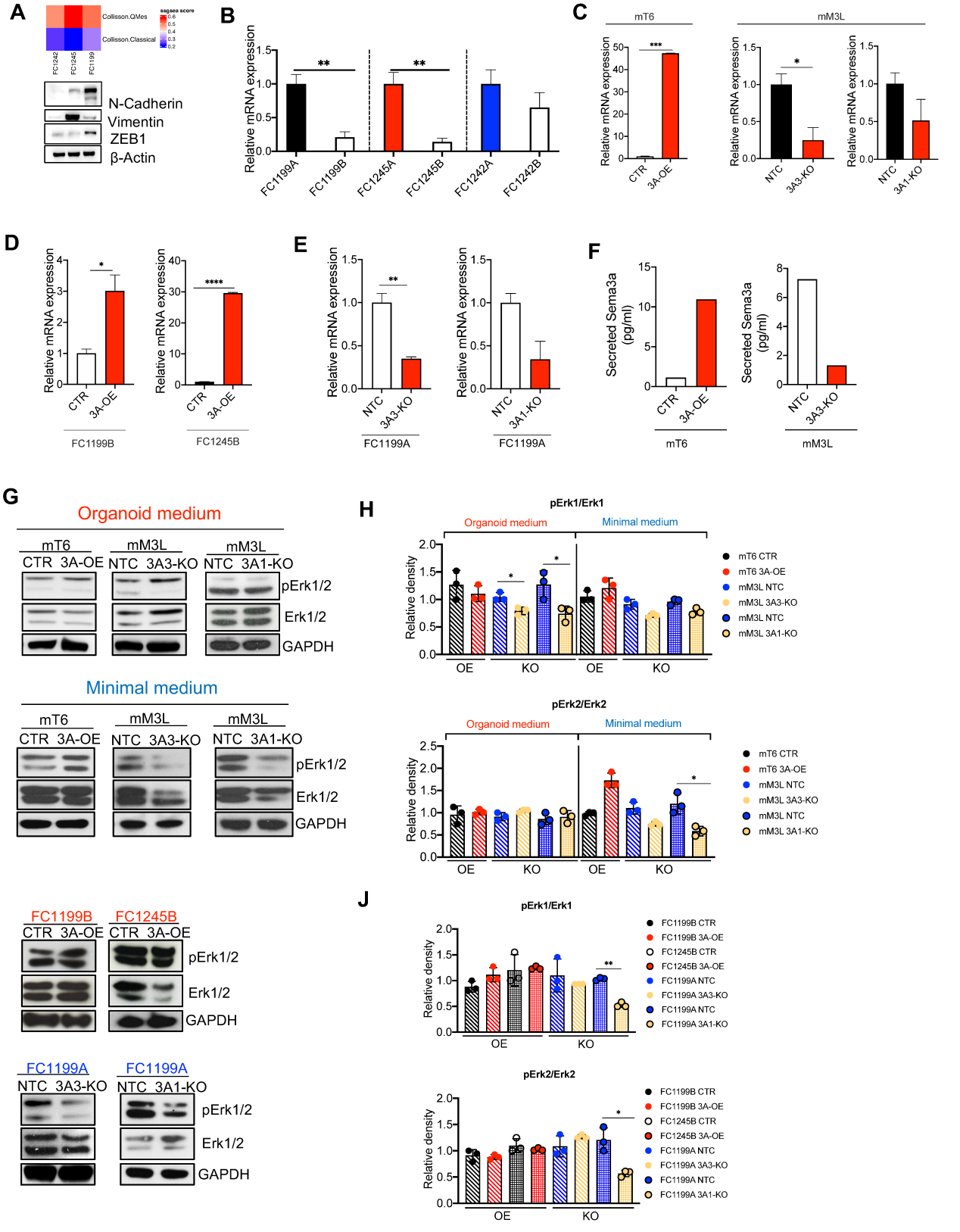
A
Collisson.QMes
Collisson.Classical
ssgsea score
FC1242
FC1245
FC1199
N-Cadherin
Vimentin
ZEB1
β-Actin
B
Relative mRNA expression
FC1199A
FC1199B
FC1245A
FC1245B
FC1242A
FC1242B
C
mT6
mM3L
CTR
3A-OE
NTC
3A3-KO
3A1-KO
D
FC1199B
FC1245B
E
FC1199A
F
Secreted Sema3a (pg/ml)
G
Organoid medium
Minimal medium
pErk1/2
Erk1/2
GAPDH
H
pErk1/Erk1
pErk2/Erk2
Relative density
OE
KO
mT6 CTR
mT6 3A-OE
mM3L NTC
mM3L 3A3-KO
mM3L NTC
mM3L 3A1-KO
I
J
FC1199B CTR
FC1199B 3A-OE
FC1245B CTR
FC1245B 3A-OE
FC1199A NTC
FC1199A 3A3-KO
FC1199A NTC
FC1199A 3A1-KO

Figure S4

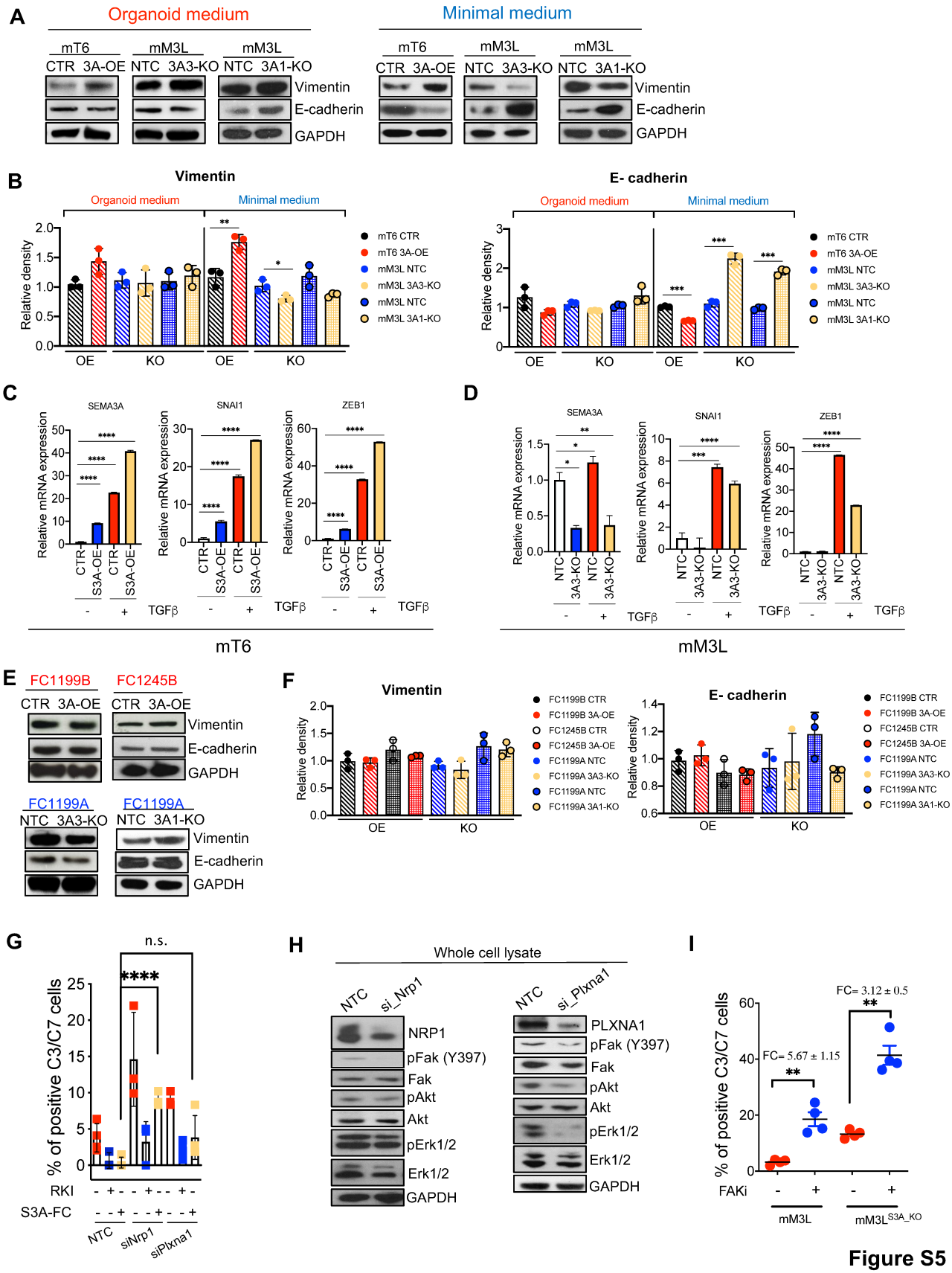
A
Organoid medium
Minimal medium
mT6
mM3L
CTR 3A-OE NTC 3A3-KO NTC 3A1-KO
Vimentin
E-cadherin
GAPDH
B
Vimentin
E- cadherin
Relative density
mT6 CTR
mT6 3A-OE
mM3L NTC
mM3L 3A3-KO
mM3L NTC
mM3L 3A1-KO
OE
KO
C
SEMA3A
SNAI1
ZEB1
Relative mRNA expression
CTR
S3A-OE
TGFβ
mT6
D
NTC
3A3-KO
mM3L
E
FC1199B
FC1245B
FC1199A
NTC 3A1-KO
F
FC1199B CTR
FC1199B 3A-OE
FC1245B CTR
FC1245B 3A-OE
FC1199A NTC
FC1199A 3A3-KO
FC1199A 3A1-KO
G
n.s.
****
% of positive C3/C7 cells
RKI
S3A-FC
NTC
siNrp1
siPlxna1
H
Whole cell lysate
si_Nrp1
si_Plxna1
NRP1
PLXNA1
pFak (Y397)
Fak
pAkt
Akt
pErk1/2
Erk1/2
GAPDH
I
FC= 5.67 ± 1.15
FC= 3.12 ± 0.5
FAKi
mM3L
mM3L S3A_KO

Figure S5

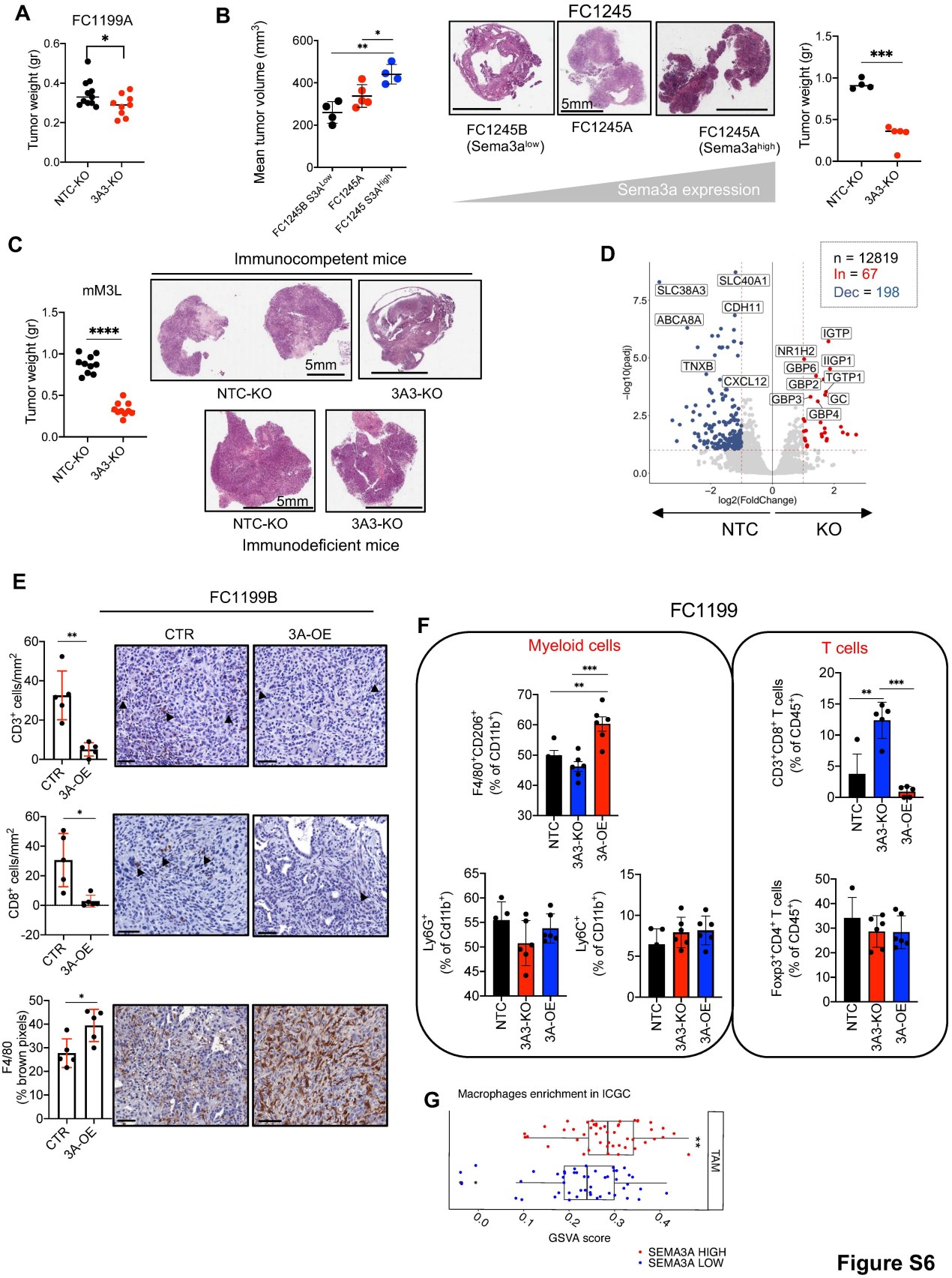
A
FC1199A
Tumor weight (gr)
NTC-KO
3A3-KO
B
Mean tumor volume (mm3)
FC1245B S3A Low
FC1245A
FC1245 S3A High
FC1245
5mm
FC1245B (Sema3a low)
FC1245A
FC1245A (Sema3a high)
Sema3a expression
Tumor weight (gr)
C
Immunocompetent mice
mM3L
Tumor weight (gr)
5mm
NTC-KO
3A3-KO
Immunodeficient mice
D
n = 12819
In = 67
Dec = 198
SLC38A3
SLC40A1
CDH11
ABCA8A
TNXB
CXCL12
IGTP
NR1H2
IIGP1
GBP6
TGTP1
GBP2
GBP3
GC
GBP4
−log10(padj)
log2(FoldChange)
NTC
KO
E
FC1199B
CTR
3A-OE
CD3+ cells/mm2
CD8+ cells/mm2
F4/80 (% brown pixels)
F
FC1199
Myeloid cells
T cells
F4/80+CD206+ (% of CD11b+)
Ly6G+ (% of Cd11b+)
Ly6C+ (% of CD11b+)
CD3+CD8+ T cells (% of CD45+)
Foxp3+CD4+ T cells (% of CD45+)
NTC
3A3-KO
3A-OE
G
Macrophages enrichment in ICGC
TAM
GSVA score
SEMA3A HIGH
SEMA3A LOW

Figure S6

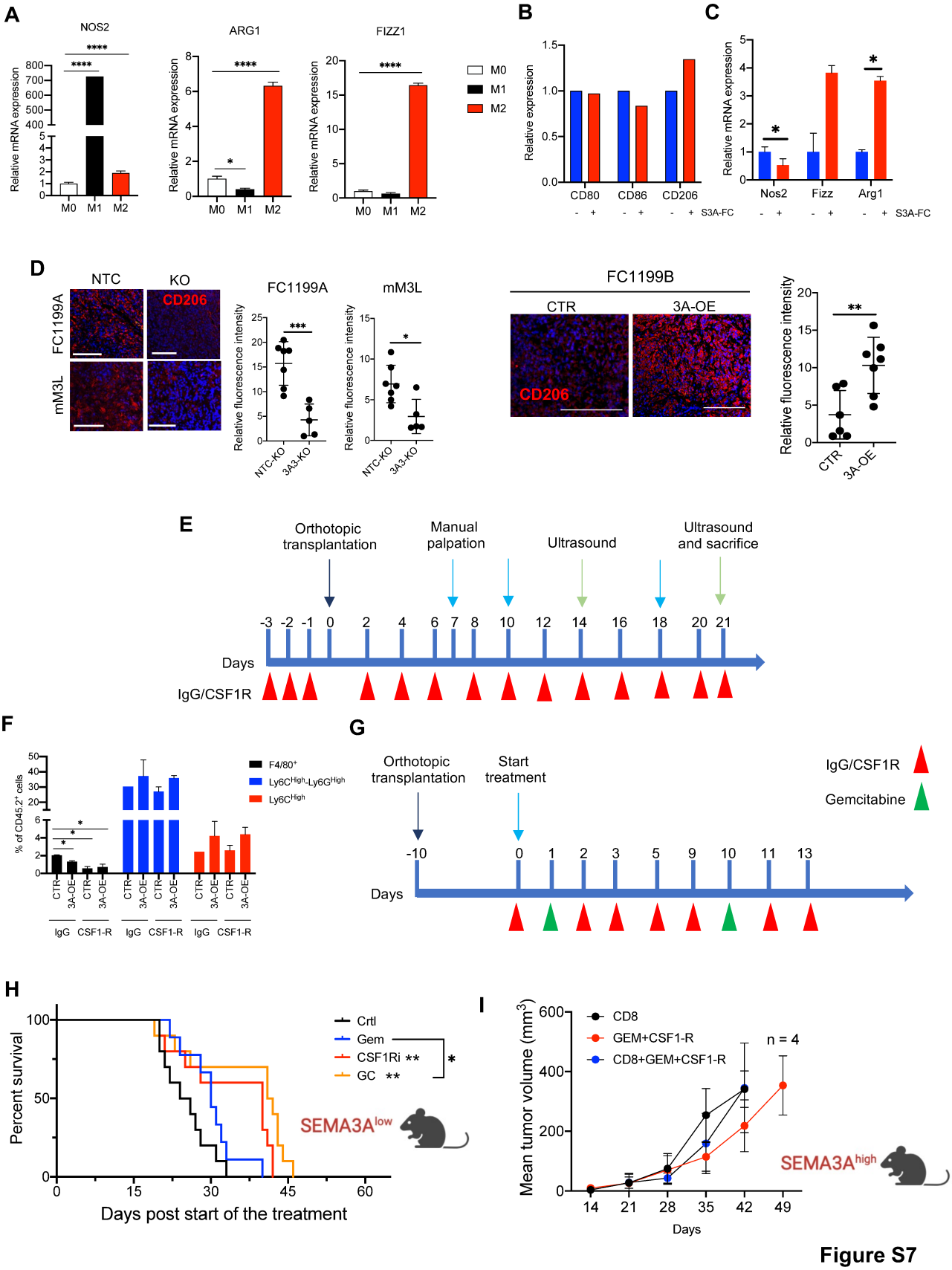
A
NOS2
ARG1
FIZZ1
Relative mRNA expression
M0
M1
M2
B
Relative expression
CD80
CD86
CD206
S3A-FC
C
Relative mRNA expression
Nos2
Fizz
Arg1
S3A-FC
D
NTC
KO
FC1199A
mM3L
CD206
Relative fluorescence intensity
NTC-KO
3A3-KO
FC1199B
CTR
3A-OE
E
Orthotopic transplantation
Manual palpation
Ultrasound
Ultrasound and sacrifice
Days
IgG/CSF1R
F
% of CD45.2+ cells
F4/80+
Ly6CHigh-Ly6GHigh
Ly6CHigh
IgG
CSF1-R
G
Orthotopic transplantation
Start treatment
IgG/CSF1R
Gemcitabine
Days
H
Percent survival
Days post start of the treatment
Crtl
Gem
CSF1Ri **
GC **
SEMA3Alow
I
Mean tumor volume (mm3)
CD8
GEM+CSF1-R
CD8+GEM+CSF1-R
n = 4
SEMA3Ahigh
Days

Figure S7